Rivista Italiana di Paleontologia e Stratigrafia
(*Research in Paleontology and Stratigraphy*)
vol. 132(3): 587-610. **November 2026**
DOI: https://doi.org/10.54103/2039-4942/31965

ANATOMY OF AN UPPER ZANCLEAN MIXED SILICI-BIOCLASTIC TRANSGRESSIVE SYSTEM: THE ROLE OF HIGH-FREQUENCY EUSTASY AND TECTONIC SUBSIDENCE ON THE STRATAL ARCHITECTURE OF THE SPUNGONE SANDSTONE, EASTERN CENTRAL ITALY

CLAUDIO DI CELMA[1], MICHELA PRINCIPI[1], ALAN PITTS[1*], JOHN T. HAYNES[2], GABRIELE GIULI[1], ELISA MALINVERNO[3], MICHELE MALAVOLTA[1], SERENA GRASSELLI[1], PIETRO PAOLO PIERANTONI[1], GIULIA BOSIO[4], GIOVANNI COLETTI[3], TIZIANO VOLATILI[1], ALESSANDRO DI MICHELE[5] & GINO CANTALAMESSA[1]

[1]School of Science and Technology, Geology Division, Università degli Studi di Camerino, Camerino, Italy. E-mail: claudio.dicelma@unicam.it
[2]Department of Geology and Environmental Science, James Madison University, Harrisonburg, VA 22807, USA
[3]Dipartimento di Scienze Dell'Ambiente e Della Terra, Università degli Studi di Milano-Bicocca, Milano, Italy
[4]Dipartimento di Scienze della Terra, Università di Pisa, Pisa, Italy
[5]Dipartimento di Fisica e Geologia, Università di Perugia, Perugia, Italy
[*]Present address: USGS, Florence Bascom Geoscience Center, Reston, VA 20192, USA

Associate Editor: Luca Martire.

To cite this article: Di Celma C., Principi M., Pitts A., Haynes J.T., Giuli G., Malinverno E., Malavolta M., Grasselli S., Pierantoni P.P., Bosio G., Coletti G., Volatili T., Di Michele A. & Cantalamessa G. (2026) - Anatomy of an upper Zanclean mixed silici-bioclastic transgressive system: The role of high-frequency eustasy and tectonic subsidence on the stratal architecture of the Spungone Sandstone, eastern central Italy. *Rivista Italiana di Paleontologia e Stratigrafia*, vol. 132(3): 587-610.

Keywords: sequence stratigraphy; shoreface cyclicity; sediment provenance; source-to-sink systems.

Abstract. The upper Zanclean Spungone Sandstone records the onset of a major transgression along the western margin of the Periadriatic Basin, eastern central Italy, and comprises a 130 m-thick succession of shallow-marine strata characterized by a highly regular cyclical stratigraphy. Integrated analysis of both physical and biogenic structures, together with the identification of major stratal surfaces and the reconstruction of the stratigraphic framework, proved essential for understanding the erosional and depositional processes that occurred during sediment deposition. Eight high-frequency depositional sequences, typically a few to tens of meters thick, have been identified based on the repetitive vertical stacking of facies associations. Sequences are bounded by low-relief erosional discontinuities recording abrupt shallowing and modest basinward shifts of facies, interpreted as amalgamated sequence boundaries formed by subaerial exposure during relative sea-level lowering and marine planation during the subsequent relative rise.

Each sequence is characterized by remarkably similar facies successions organized in a deepening-upward pattern and interpreted as transgressive systems tracts, partially truncated by erosional beveling at the overlying sequence boundary. Deposits attributable to the highstand and falling-stage systems tracts are absent, an architectural style typical of depositional sequences formed in low-accommodation basin-margin settings. Patterns in facies composition are suggestive of deposition in shoreface settings under storm conditions of varying intensity, revealing two fundamental types of sedimentary motif: weakly storm-affected and strongly storm-dominated shorefaces. The overall sequence-stratigraphic organization of the Spungone Sandstone exhibits an aggradational stacking pattern of component sequences, suggesting that they were almost certainly generated by high-rate, small-amplitude glacio-eustatic sea-level fluctuations superimposed on lower rate, tectonically-induced subsidence.

Petrographic analysis of these well-sorted mixed siliciclastic-carbonate sandstones indicates that the bioclastic component mainly consists of skeletal debris derived from a contemporaneous cool-water carbonate factory. The terrigenous fraction is instead dominated by limestone lithic fragments, chert, and metamorphic quartz that were sourced from the progressive unroofing of the Mesozoic-Cenozoic cherty limestones of the Umbria-Marche domain and the Messinian turbiditic sandstones of the Laga Formation exposed in the uplifted Apennine sectors west of the study area.

Received: June 23, 2026; accepted: August 28, 2026

Introduction

Shallow-water settings represent a critical component of source-to-sink systems, occupying a narrow, high-energy transitional zone within the continuum that links sediment production in source regions, sediment transfer zones, and deposition in the ultimate deep-marine sinks (Castelltort et al. 2023 and references therein). They form a highly dynamic and responsive system controlling cross-shore sediment transfer over multiple timescales and play a key role in controlling the volume, grain size, and timing of sediment flux delivered to the receiving basin (e.g., Anthony & Aagaard 2020).

Even under conditions of intense reworking, the compositional signature of shallow-water deposits commonly retains a recognizable connection to their source areas, with mineralogical assemblages and grain types reflecting the nature of the hinterland and the lithologies exposed within the drainage basin (e.g., Mazumder 2017). This relationship is rarely straightforward, as down-system selective transport, longshore drift, hydraulic sorting, and abrasion can significantly modify primary signals (e.g., Okwara et al. 2025). Nevertheless, shallow-water deposits often preserve a filtered but still informative record of sediment provenance (Van Loon et al. 2017; Coletti et al. 2025), providing an important link between upstream source regions and downstream depositional systems. At the same time, shallow-water settings exert a strong control on sediment texture through selective transport processes. Wave action and longshore currents promote efficient sediment sorting and partitioning of grain sizes, commonly favoring the retention of coarser fractions within the littoral domain while facilitating the offshore transfer of finer particles. As a consequence, the sediment that ultimately reaches deeper marine settings is not a simple reflection of source characteristics, but the result of substantial modification within the terrestrial and shallow-water systems (e.g., Bouma & Scott 2003; Sømme et al. 2009; Allen et al. 2017; Marsaglia et al. 2026).

From a stratigraphic perspective, nearshore and inner shelf deposits are highly sensitive indicators of relative sea-level fluctuations and variations in sediment supply, thus providing valuable archives for reconstructing shoreline dynamics and environmental change (e.g., Nalin et al. 2007; Bizzarri 2010; Rousse et al. 2012). A significant body of outcrop-based studies of Pliocene-Pleistocene shallow-marine successions have shown that these deposits record variations in ice caps volumes as well-defined cyclothemic patterns that require a facies-based sequence stratigraphic framework to be properly interpreted (e.g., Clifton et al. 1988; Collier 1990; Ito & Katsura 1992; Kitamura et al. 1994; Saul et al. 1999; Pomar & Tropeano 2001; Cantalamessa & Di Celma 2004; Cantalamessa et al. 2005; Di Celma et al. 2005a, b; Ghinassi 2007; Massari & D'Alessandro 2010; Zecchin et al. 2022, 2025a).

The study reported here focuses on a Lower Pliocene shallow-marine mixed bioclastic-siliciclastic succession (Spungone Sandstone) from the Periadriatic Basin, eastern central Italy, providing a clear example of warm-temperate shallow-marine sedimentation controlled by external (allogenic) factors, such as climatic conditions, high-frequency glacio-eustatic sea level changes, sediment supply, and tectonic subsidence. The preserved stratigraphic succession represents a partial record of a "steep, short, and deep" sediment-routing system (Helland-Hansen et al. 2016), with its upstream portion (the alluvial and fluvial transfer zone) no longer preserved due to uplift and erosion and its distal portion (the offshore depositional basin) buried and inaccessible for study. Assessing sediment provenance and understanding these external controls, their magnitude, and their interactions is essential for linking the mountainous source terrains to downstream segments of the sediment-routing system (e.g., Nayak et al. 2022), as well as for reconstructing and predicting how sediment has been transported, temporarily stored (and in part permanently sequestered) in shallow-water settings, and ultimately delivered to the deepwater subsurface sink through time, thereby contributing to establish a foundation for future source-to-sink studies in the Periadriatic Basin.

The present study is chiefly directed at: i) outlining a robust facies scheme for the Spungone Sandstone; ii) establishing a detailed, high-resolution sequence stratigraphic framework by identifying key discontinuity surfaces and genetic stratigraphic units; and iii) providing a refined account of its petrographic signature needed to establish the potential sediment sources.

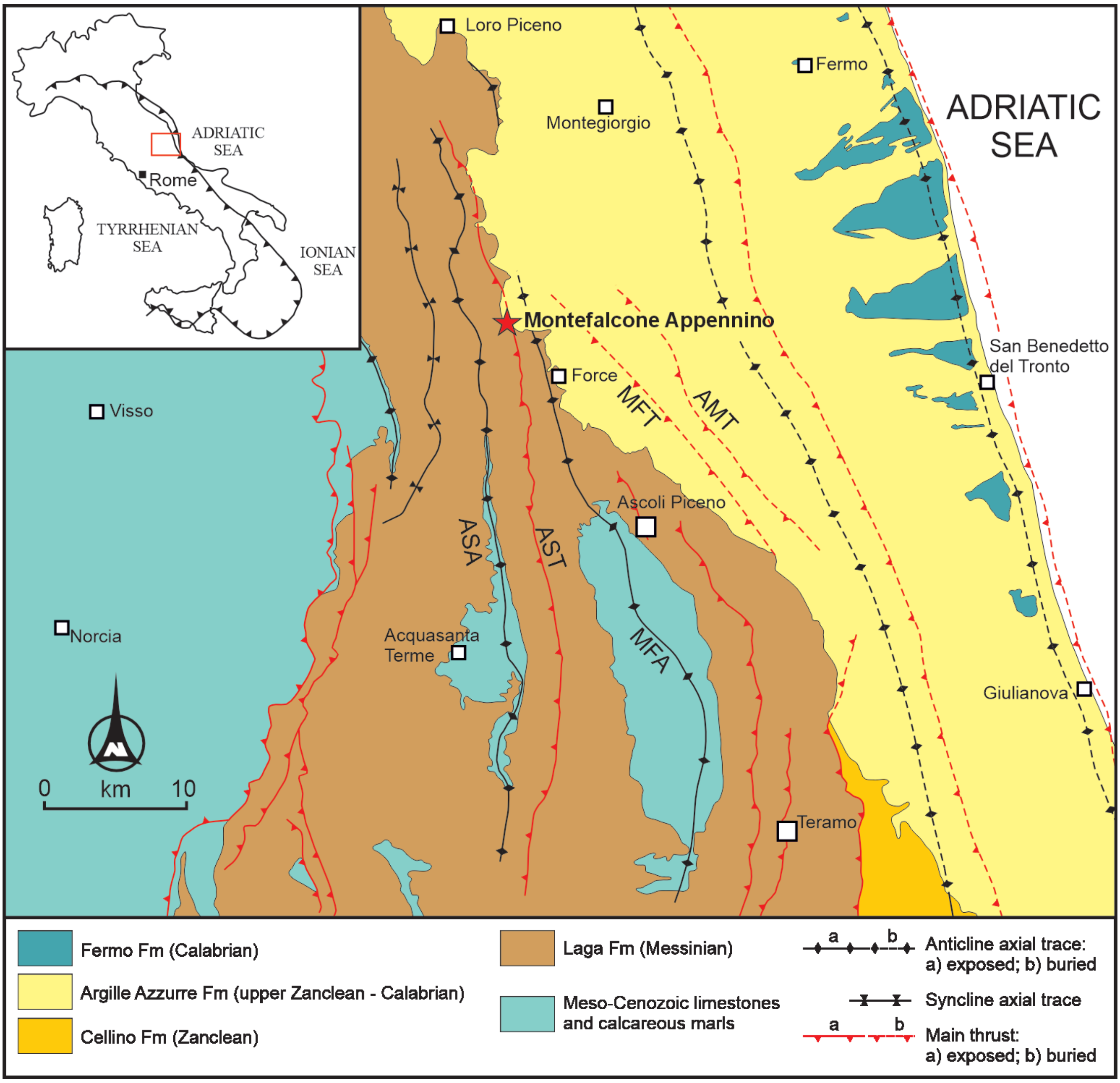

Fig. 1 - Simplified geological map of southern Marche and northern Abruzzo regions in eastern central Italy (see red rectangle in the top left inset for location) with the distribution of the main stratigraphic units and indication of the locality discussed in this study. ASA, Acquasanta Anticline; MFA, Montagna dei Fiori Anticline; AT, Appignano Thrust; AST, Acquasanta Thrust; MFT, Montagna dei Fiori Thrust.

Geological setting and stratigraphy

The southern sector of the Northern Apennines is a NW-SE-trending, east-verging fold-and-thrust belt that has developed since the late Oligocene as a consequence of the westward subduction of the Adria microplate beneath the European plate (e.g., Malinverno and Ryan 1986; Dewey et al. 1989; Patacca et al. 1990; Boccaletti et al. 1990; Doglioni 1991). During the Oligocene-Miocene collision, tectonic accretion, thrust-sheet loading, and the eastward rollback and retreat of the subducting Adria slab (e.g., van der Meulen et al. 1998, 2000) led to the development of an eastward-migrating foreland basin system (sensu De Celles 2012) including a set of asymmetric foredeeps and associated piggy-back basins (Ori & Friend 1984; Ricci Lucchi 1986; Argnani & Ricci Lucchi 2001). In this frame, during the Messinian the study area was an elongate, north-south-striking foredeep that filled with the thick turbiditic succession of the Laga Formation (Fig. 1). This unit displays a clear bipartite stratigraphic organization, comprising a lower sand-rich portion (ME supersynthem in Fig. 2A) fed by a large Alpine source area (Stalder et al. 2018), and an upper mud-rich portion (ME3 synthem in Fig. 2A) fed by relatively smaller Apennine source areas (Valloni et al. 2002).

During the late Messinian and the Pliocene, the Laga foredeep basin experienced major phases of deformation and depocenter migration, commonly associated with active thrusting and the development of new, more external thrust systems (Ori et al. 1993; Bigi et al. 2011; Artoni 2013; Pedini et al. in press). The foredeep was fragmented, its sediments were incorporated into the north-south-trending Apennine fold-and-thrust belt, and its depocenter migrated into a more external position (i.e., eastward), leading to the development of two distinct depozones that received sediments from the uplifting orogen to the west: i) the inner piggy-back Periadriatic Basin; and ii) the more external Adriatic foredeep.

Several regional stratigraphic studies have aimed to unravel the complexities of the Messinian-Pleistocene deposits filling the central Apennine foreland system, whose tectonostratigraphic history is recorded by basin-wide unconformities of variable duration (Fig. 2A) that document discrete phases of structural deformation and basin development (Crescenti et al. 1980, 2004; Casnedi 1983; Ori et al. 1993; Centamore et al. 1992, 2003; Bigi et al. 1999, 2013; Dattilo et al. 1999; Cantalamessa et al. 2002; Crescenti et al. 2004; Carruba et al. 2006; Artoni 2007, 2013; Ghielmi et al. 2019; Di Celma et al. 2023). These events triggered the migration of foredeep depocenters toward the foreland and correspond to changes in basin configuration, as well as in the type and spatial distribution of depositional systems (Ori et al. 1993; Tozer et al. 2006; Artoni 2013).

During the Pleistocene, eastern central Italy has been uplifted and exhumed to expose extensive outcrops of the Pliocene and Pleistocene Argille Azzurre Formation, which covers the outer part of the present Apennines chain-foredeep-foreland system and records the last deformation phases associated with the migration of the Apenninic orogen. Owing to the exceptional quality of outcrop exposure, its Pleistocene portion has been the focus of a number of sedimentological and stratigraphic studies, providing a detailed picture of the depositional history of the Periadriatic Basin during this period. It consists of sediments deposited in a variety of environmental settings, including shelf-slope mudstones and submarine canyon and channel fill conglomerates and sandstones (Di Celma 2011; Di Celma & Cantalamessa 2012; Di Celma et al. 2010, 2013, 2014), shallow-marine sandstones and conglomerates (Cantalamessa et al. 1986; Ori et al. 1991; Cantalamessa & Di Celma 2004; Di Celma et al. 2020; Massari 2021), and alluvial conglomerates (Di Celma et al. 2015). In contrast, little work has targeted specific depositional systems within the Pliocene portion of the basin fill, and consequently far less is known about the sedimentology, stratigraphic architecture, and composition of these strata. To address this knowledge gap, the present study is concerned with the Spungone Sandstone of the Argille Azzurre Formation, the basal part of the PL2.2 subsynthem (Fig. 2A) exposed in the southern Marche region (Di Celma 2025). This sediment wedge consists of shallow-marine pebbly and cobbly sandstones, which are overlain by, and grade laterally eastward into, deeper-water, offshore hemipelagic mudstones of the Argille Azzurre Formation (Cantalamessa et al. 1986; Ori et al. 1991; Ghielmi et al. 2019). As a whole, it represents the leading edge of the late Zanclean transgression in this region, where it forms a belt of variously exposed, north-south-trending vertical escarpments between the villages of Loro Piceno to the north

Fig. 2 - A) Stratigraphic scheme of the Miocene to Pleistocene sedimentary succession of the central Apennine foredeep. Mediterranean planktonic foraminiferal and calcareous nannofossil biozonal schemes modified after Lirer et al. (2019) and Di Stefano et al. (2023), respectively. UBSU-based stratigraphic subdivision is based on regional unconformities produced by basin-wide modifications related to major compressional tectonic phases (modified after Di Celma et al. 2023 and Di Celma 2025 and references therein). Color code for the lithostratigraphic units as in Figure 1. B) Schematic east-west cross-section (not in scale) describing the main structural and stratigraphic features of the Messinian to Zanclean succession of the Apennine foredeep system exposed in the study area (derived from seismic and field data of Ori et al. 1991; Servizio Geologico d'Italia 2025; Pedini et al. 2025). C) Synthetic sedimentological log of the upper Zanclean Spungone Sandstone exposed at Montefalcone Appennino summarizing the vertical distribution of facies associations and key stratal surfaces. Cyclic variations in facies associations reflect periodic fluctuations of sea level. Black arrows indicate position of the collected samples.

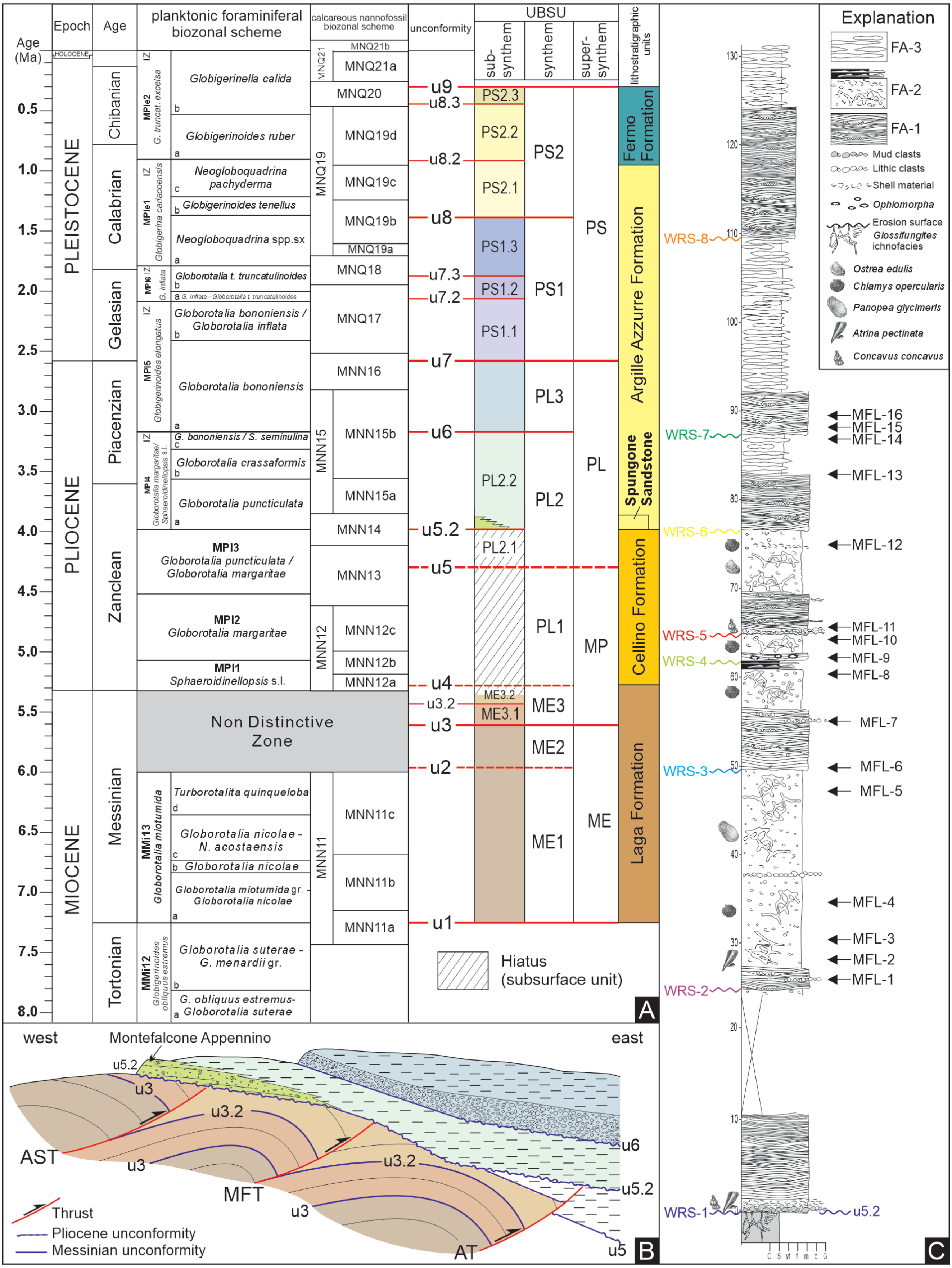
Age (Ma)
Epoch
Age
planktonic foraminiferal biozonal scheme
calcareous nannofossil biozonal scheme
unconformity
UBSU
sub-synthem
synthem
super-synthem
lithostratigraphic units
PLEISTOCENE
PLIOCENE
MIOCENE
HOLOCENE
Chibanian
Calabrian
Gelasian
Piacenzian
Zanclean
Messinian
Tortonian
Globigerinella calida
Globigerinoides ruber
Neogloboquadrina pachyderma
Globigerinoides tenellus
Neogloboquadrina spp.sx
Globorotalia t. truncatulinoides
Globorotalia bononiensis / Globorotalia inflata
Globorotalia bononiensis
G. bononiensis / S. seminulina
Globorotalia crassaformis
Globorotalia puncticulata
MPl3
Globorotalia puncticulata / Globorotalia margaritae
MPl2
Globorotalia margaritae
MPl1
Sphaeroidinellopsis s.l.
Non Distinctive Zone
Turborotalita quinqueloba
Globorotalia nicolae - N. acostaensis
Globorotalia nicolae
Globorotalia miotumida gr. - Globorotalia nicolae
Globorotalia suterae - G. menardii gr.
G. obliquus estremus- Globorotalia suterae
MNQ21b
MNQ21a
MNQ20
MNQ19d
MNQ19c
MNQ19b
MNQ19a
MNQ18
MNQ17
MNN16
MNN15b
MNN15a
MNN14
MNN13
MNN12c
MNN12b
MNN12a
MNN11c
MNN11b
MNN11a
u9
u8.3
u8.2
u8
u7.3
u7.2
u7
u6
u5.2
u5
u4
u3.2
u3
u2
u1
PS2.3
PS2.2
PS2.1
PS1.3
PS1.2
PS1.1
PL2.2
PL2.1
ME3.2
ME3.1
PS2
PS1
PL3
PL2
PL1
ME3
ME2
ME1
PS
PL
MP
ME
Fermo Formation
Argille Azzurre Formation
Spungone Sandstone
Cellino Formation
Laga Formation
Hiatus (subsurface unit)
A
west
Montefalcone Appennino
east
u5.2
u3
u3.2
AST
u3
MFT
u3.2
u6
u5.2
u3
AT
u5
Thrust
Pliocene unconformity
Messinian unconformity
B
Explanation
FA-3
FA-2
FA-1
Mud clasts
Lithic clasts
Shell material
Ophiomorpha
Erosion surface
Glossifungites ichnofacies
Ostrea edulis
Chlamys opercularis
Panopea glycimeris
Atrina pectinata
Concavus concavus
WRS-8
WRS-7
WRS-6
WRS-5
WRS-4
WRS-3
WRS-2
WRS-1
u5.2
MFL-16
MFL-15
MFL-14
MFL-13
MFL-12
MFL-11
MFL-10
MFL-9
MFL-8
MFL-7
MFL-6
MFL-5
MFL-4
MFL-3
MFL-2
MFL-1
C

Fig. 2

and Force to the south. In the study area, outcrops of the Spungone Sandstone are limited. However, they are superbly exposed in vertical cliffs along the Montefalcone Appennino escarpment, providing an oblique dip section that offers a unique opportunity to investigate patterns in facies distribution and the complexity of the stratigraphic architecture. At this locality, the Spungone Sandstone is exposed along a laterally continuous cliff over 1.5 km long and up to 130 m high. The succession rests unconformably on the folded mud-rich strata of the Laga Formation and is exposed at the northern terminations of anticlines in the hanging wall of the Acquasanta and Montagna dei Fiori thrusts (Fig. 2B). A generalized sedimentological section is shown in Figure 2C.

Direct chronostratigraphic data for the Spungone Sandstone are uncertain and dating largely relies on the age of the overlying sediments. The calcareous nannofossil and planktonic foraminiferal assemblages recovered from the immediately overlying portion of the offshore mudstones of the Argille Azzurre Formation (42°59'5.5"N, 13°29'3.5"W) are generally sparse and poorly preserved. Nevertheless, the co-occurrence of diagnostic species such as *Reticulofenestra pseudoumbilicus* (Gartner 1967) Gartner, 1969 and *Pseudoemiliana older* Kamptner, 1963 ex Gartner 1969, together with *Globorotalia puncticulata* (Deshayes 1832) and rare specimens of *Globorotalia margaritae* Bolli and Bermudez 1965, allow to assign this interval to the calcareous nannofossil Biozone MNN14 of Di Stefano et al. (2023) and to the lower part of the planktonic foraminiferal *Globorotalia puncticulata* Subzone (MPl4a) of Lirer et al. (2019). Based on these biostratigraphic constraints, the age of the underlying Spungone Sandstone is estimated at approximately 4 Ma or slightly older, corresponding to the late Zanclean.

Methods

The Spungone Sandstone stratigraphy described herein is exposed along the Montefalcone Appennino escarpment where a reference stratigraphic section was measured at cm-scale along the roadcut exposure that bisects the escarpment (Fig. 2C). Field data were obtained using conventional methodology of logging and collecting information on the macroscopic features of the succession, including textural characters, composition, primary sedimentary structures, skeletal components, ichnological features and amount of bioturbation, bed thickness, and nature of bounding contacts. Grain size was estimated in the field using a hand lens and a grain-size comparator card. Degree of bioturbation was evaluated following the simplified four-fold bioturbation index (BI) scheme of Taylor and Goldring (1993): no bioturbation (BI = 0), low (BI = 1), moderate (BI = 2-3) and high bioturbation (BI = 4-6). Subdivision of the Spungone Sandstone into distinct facies associations (FA-1, FA-2, and FA-3) was achieved through the identification of characteristic physical and biogenic sedimentary features observed directly in outcrop. While measuring the section, sixteen sandstone samples (named MFL1 to MFL16 in Fig. 2C) were collected to be processed for petrological, XRD, and SEM analyses.

Traditional outcrop data obtained via field-based analysis were complemented by imagery obtained using Unmanned Aerial Vehicle (UAV) and Structure-from-Motion multi-view stereo photogrammetry (SfM-MVS), which facilitated detailed examination of the cliff faces, where facies associations are often enhanced by differential weathering, by generating detailed 3D photogrammetry outputs (i.e., georeferenced point cloud, and textured mesh). Results were integrated to produce detailed outcrop mapping, enabling reconstruction of the stacking pattern and development of a facies- and sequence stratigraphy-based depositional model. A DJI Mavic 3 Classic drone, equipped with a camera having a CMOS 4/3" 20 MP sensor, was deployed to collect 568 photos. These images were acquired at a flight altitude of 60 m above ground level with a frontal and side overlap of 70% and 50%, respectively. The photos were processed into three-dimensional digital outcrop models following well-established procedures using Agisoft Metashape PRO (James & Robson 2012; Pitts et al. 2017; Nesbit 2018; Over et al. 2021; Seers et al. 2022). These models provided photo-realistic and georeferenced three-dimensional Virtual Outcrop Models (VOMs) of the entire outcrops, generating a point cloud of 437,670 points and high-quality dense clouds. Meshes were created using a medium face count setting, resulting in final texture models composed of 63,611,398 faces. The VOMs proved particularly useful for correlating stratal surfaces along inaccessible cliff faces, defining stratal lap-out patterns, and characterizing facies distribution and stratigraphic framework. Initial analysis of the VOMs data was done inside Agisoft Metashape using the 3D polyline tool functionality. The outcrop model was subsequently exported as a .LAZ file into CloudCompare v2.13 beta software (Thiele et al. 2017) for further interpretation and extraction of quantitative and qualitative geological data. This included: i) measuring the thickness of individual high-frequency sequences and their component facies associations along the vertical face of the escarpment; and ii) tracing and characterizing key stratal surfaces based on facies-association stacking patterns and the interpretation of lap-out relationships.

Sixteen thin sections tied to key stratigraphic intervals were examined under a standard petrographic microscope and assessed for grain and matrix composition, fossil content, grain-population distribution, and texture. In this case a binocular Euromex (Holland) microscope was used with 4x, 10x, 16x objectives. Seven of the sixteen thin sections were stained using the standard Dickson method (Dickson 1965) to distinguish ferroan calcite from non-ferroan calcite, and ferroan dolomite from non-ferroan dolomite. These seven thin sections were also point counted (300 framework grains each) to determine detrital modes of the sand fraction using an Olympus BX50 petrographic microscope with 4x, 10x, 20x, and 40x objectives and an attachable point counting mechanical stage. Mineral identification and their relationships were based on the petrographic characteristics, crystal shape, orientation, and diagenetic alteration.

Samples for Powder X-Ray Diffraction analysis were finely ground using a mullite mortar to obtain a homogeneous fine-grained powder. Each sample was then mounted in a brass sample holder by side loading in order to minimize grain preferred orientation, which could otherwise affect the relative intensities of the diffraction peaks. Step scan powder diffraction data were recorded for each sample using an automated PHILIPS diffractometer equipped with diffracted-beam soller slits, 1° divergence-slits, 0.1 mm receiving slits and a graphite diffracted-beam monochromator. The Cu X-ray tube was operated at 40 kV and 25 mA. The spectra were recorded in the 2-theta range from 3° to 75° with a 0.02° step and 5 seconds counting time. For each diffractogram, peak position has been converted to interplanar distances, and the resulting values have been compared with the PDF database (Kabekkodu et al. 2024).

Additional mineralogical information was gathered using scanning electron microscopy-energy-dispersive spectrometry, and backscatter electron images were collected to illustrate key compositional features. The thin sections previously used for optical microscopy were carbon-coated and analyzed using a field-emission scanning electron microscope (FE-SEM; Zeiss LEO 1525) to obtain semiquantitative data on chemical composition. Imaging was performed with an angle-selective backscattered electron detector (AsB) and an in-lens secondary electron detector, and chemical analyses were acquired using a Bruker Quantax 200 EDX system equipped with an X-Flash 410 detector. The SEM was operated at 15 kV voltage, to be able to easily detect also the Fe, Co and Ni K-alpha emission lines. Backscattered electron images have been used to discriminate the minerals present in each field of view. EDX spectra have been processed by means of an Espirit 1.9 software using ZAF correction to derive elemental abundances and elemental maps have also been collected to try ascertaining the presence of compositional zonation in the minerals of interest.

In situ U-Pb dating of detrital zircons was performed by laser ablation using the inductively coupled plasma-mass spectrometer (LA-ICP-MS) on polished standard petrographic thin sections. Analyses were undertaken at the University of Perugia and the analytical instrumentation used in this study is described in Alagna et al. (2008).

Results

This section presents the results of the sedimentologic, petrographic, and mineralogical analyses and forms the basis for an interpretation of the Spungone Sandstone in the context of fluctuations of relative sea level and reconstruction of the potential source areas.

Facies Analysis

The Montefalcone succession consists of a cyclic stack of shoreface deposits truncated by a series of laterally extensive erosional discontinuities. These surfaces bound stratal units whose internal architecture comprises three main facies associations, interpreted as deposits of middle shoreface settings (FA-1) and, depending on storm intensity and frequency (MacEachern & Pemberton 1992; Pemberton et al. 2012), of either weakly storm-affected lower shoreface settings (FA-2) or strongly storm-dominated lower shoreface settings (FA-3). The shoreface is defined as the part of the seafloor between mean low tide and the fair-weather wave base (i.e., Galloway & Hobday 1996; Reading & Collinson 1996; Plint 2010; Pemberton et al. 2012). Details of each are discussed and interpreted below.

Interlayered finely laminated sandstones and conglomerates (FA-1 - middle shoreface): This facies association forms sedimentary packages ranging from 2.5 to 15 m in thickness. Its basal contact is invariably sharp and scoured, locally burrowed by a *Glossifungites* Ichnofacies, and may be marked by the accumulation of a conglomerate layer of well-rounded extrabasinal pebbles and small cobbles or mud rip-up clasts ranging in thickness from one-clast to several decimeters. In one case (Sequence 1), this conglomerate layer is overlain by a dispersing-upward shellbed that is dominated by bivalves and barnacles occurring in a variety of preservation states ranging from broken shells to disarticulated and articulated specimens. Individual sandstone beds display a broadly tabular geometry and show a uniform thickness over lateral distances of several tens of meters, before thinning markedly and onlapping onto the underlying stratal surface in a paleo-landward (i.e., westward) direction. Beds have sharp bases, range from a few centimeters to several decimeters in thickness and occur primarily in amalgamated bedsets. Very thin, granule- and small pebble-size conglomerate interbeds and medium-bedded, lenticular conglomerates are common, particularly at the base of low-angle internal scours (Fig. 3A). Although sedimentary structures are typically difficult to discern, finely plane-parallel and quasi-planar-laminated (0.5-2 mm) sandstone beds can be recognized (Fig. 3B, C). The quasi-planar lamination exhibits a subtle yet perceptible undulation and shows no evidence of lateral accretion, but only vertical aggradation. Body fossils are not generally common, and where present they are often fragmentary and thinly spread on the laminae. Bioturbation is sporadic and unevenly distributed, with bioturbation index ranging from absent to moderate (BI = 0-3). Observed trace fossils include occasional horizontal or sub-horizontal knobby-walled *Ophiomorpha* (Fig. 3D). Fossil leaves occur sporadically along plane-parallel laminae within the sandstone beds.

Within the conglomerates and pebbly and cobbly sandstones, clasts are invariably well rounded and consist of various lithologies, including lime mudstones, packstones, and grainstones, and black and red chert pebbles and cobbles derived from the Mesozoic-Cenozoic successions exposed in the adjacent Apennine orogenic wedge. These clasts occur as thin, discrete stringers of small pebbles of relatively uniform size, as small clusters within depressions along undulatory amalgamation surfaces, or as scattered isolated small pebbles and granules (Fig. 3A). Interstratified conglomerates also occur as laterally discontinuous, broadly lenticular, massive beds up to 40 cm thick that are characterized by a sharp, undulating basal contact, a matrix-supported fabric and a medium to fine sandy matrix (Fig. 3E). In those conglomeratic beds, mean clast size ranges from 2 to 8 cm in diameter, although finer- (e.g., granule-grade) and coarser-grained (coarse cobble-grade) clasts are also present.

The occurrence of marine skeletal remains, together with the relatively coarse grain size, diagnostic sedimentary structures, general dearth of trace fossils, and absence of muddy and silty interlayers, indicates deposition of this facies association above the fair-weather wave base in a mid-

Fig. 3 - Representative outcrop photographs of the interlayered middle shoreface sandstone and conglomerate deposits (FA-1) and their common sedimentological and ichnological features. A) General view of broadly horizontally stratified, finely laminated sandstones interpreted as amalgamated storms beds. Granule- or pebble-size clasts are segregated into discrete, laterally discontinuous, thin conglomerate beds (white arrows). B) Detail of quasi-planar-laminated sandstone beds (QPL). Note the subtle, gentle undulation of internal millimeter-scale lamination. Note also the knife-sharp erosional contact, mantled by a thin veneer of extrabasinal pebble- to granule-sized clasts (black arrow), representing a transgressively modified sequence boundary (WRS-3) (position of this image is provided in Figure 6C). C) Close-up showing faintly plane-parallel laminated sandstones with small, isolated granules. A 14 cm-long marker for scale. D) Vertical face showing pellet-lined horizontal *Ophiomorpha* (Op) traces in fine- to medium-grained sandstones. E) Detail of dispersed pebble clasts, continuous to discontinuous granule- to pebble-sized stringers, and interstratified lenses of matrix-supported pebble conglomerate and sandstone. A 13 cm-long black marker for scale.

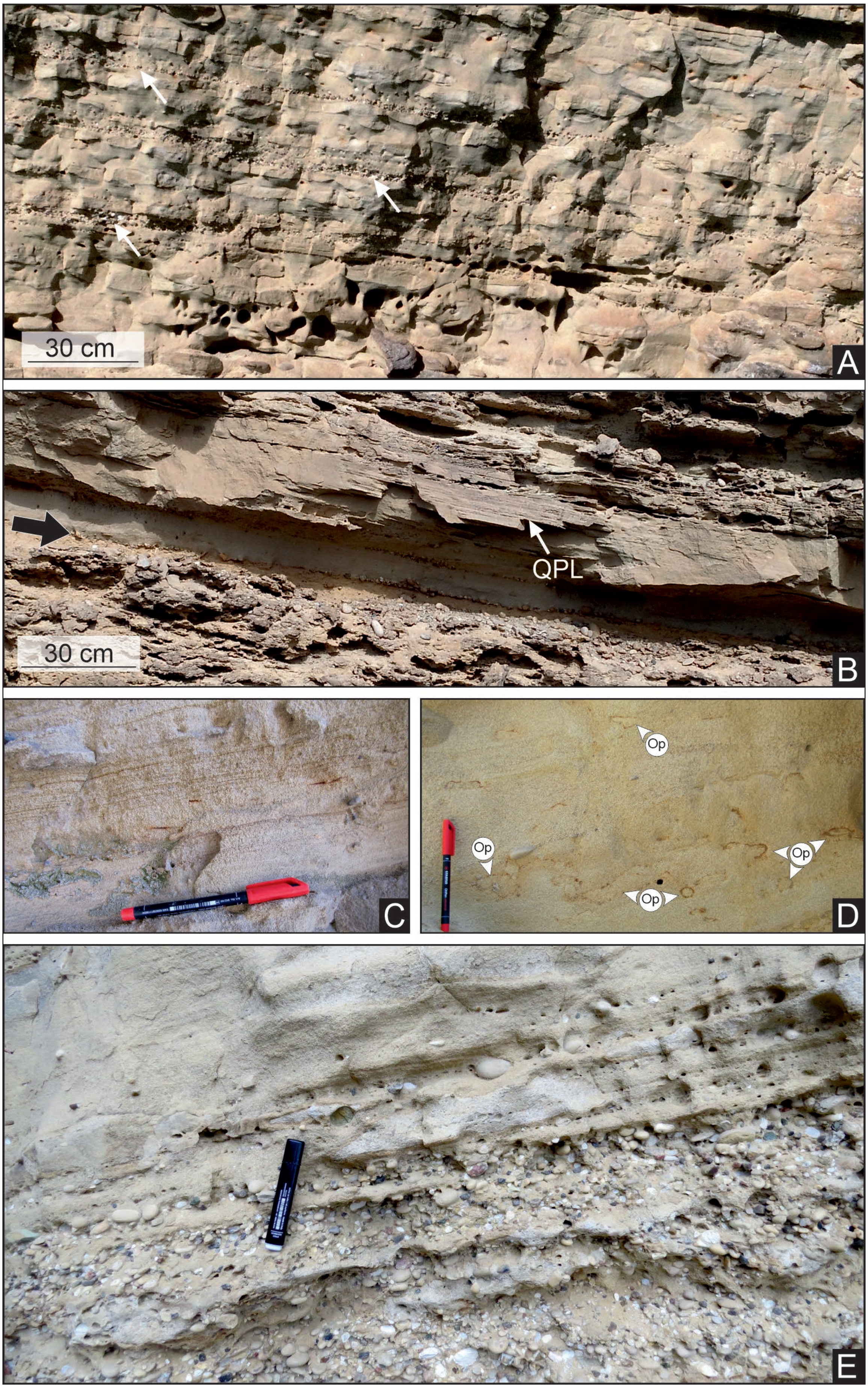

Fig. 3

dle shoreface setting, probably under high-energy combined-flow conditions. This interpretation is supported by the dominance of plane-parallel and quasi-planar lamination, which are indicative of oscillatory-dominated combined flows with high aggradation rates during storm events (e.g., Arnott 1993; Hill et al. 2003; Jelby et al. 2020). Under such conditions, storm-related currents and waves distributed both extrabasinal siliciclastics and intrabasinal bioclasts under a physical regime characterized by net offshore sediment transport. The presence of barnacle remains in a variable preservation state, including fragmented specimens, is also suggestive of a shallow-water coastal high energy setting (Coletti et al. 2021, 2024). A restricted suite of dwelling structures, dominated by the presence of horizontal *Ophiomorpha* burrows, is indicative of the activity of opportunistic trace makers that colonized the sandy substrate shortly after sand deposition (Pemberton et al. 1992; MacEachern & Bann 2008). The presence of thin layers of extrabasinal pebbles records repeated reworking by waves and/or longshore currents under storm conditions (Clifton 2003). This material was probably supplied by a nearby river and transported offshore by seaward-directed rip currents during or immediately after storm events, as well as deposited within longshore troughs (e.g., Bourgeois & Leithold 1984; Nemec & Steel 1984; Hart & Plint 1995).

Based primarily on their position directly overlying interpreted transgressively modified sequence boundaries (discussed below), the conglomerate layers, which are locally rich in shells as commonly observed along the basal erosional discontinuities, are best regarded as ravinement-reworked lag deposits formed during shoreface retreat. Transgressive lags form through the exhumation and redistribution of pre-existing sediments (e.g., Zecchin et al. 2017, and references therein; Puig López & Howell 2024), and they typically represent significant time intervals and multiple episodes of reworking by various processes, chiefly storm waves and currents, resulting in sediment bypassing and winnowing.

Thoroughly bioturbated pebbly sandstones (FA-2 – weakly storm-dominated lower shoreface): This facies association forms sedimentary packages ranging from about 3 to 22 m in thickness and consists of a thoroughly bioturbated mixture of fine- to coarse-grained sandstones, shell fragments, and lithic pebbles (up to 8 cm in size) scattered throughout the section with no apparent sorting or organization (Fig. 4A, B). Thin granule to pebble stringers may be present but they are uncommon and typically biogenically disrupted. Bedding, sedimentary structures, and trace fossils are very difficult to identify as a result of the intense and widespread biogenic reworking (BI = 5-6), although some relict planar lamination and wavy lamination associated with penecontemporaneous soft-sediment deformation is present locally. The intense biogenic reworking results in crumbly, weakly cemented, and weathered deposits. The skeletal assemblage is composed of a rich association of shallow-water bivalves and gastropods (Mascarini 1880), locally associated with barnacles, brachiopods, echinoids, decapod crustacean fragments, and other taxa (Table 1). Bivalves are generally dispersed within the sand, preserved either as entire shells or as disarticulated and broken valves, but in some beds densely to loosely packed, monospecific or low-diversity concentrations of disarticulated, flat-lying shells (Fig. 4C), up to 30 cm thick, are present. Specimens of the deep-burrowing *Panopea glycimeris* (Born, 1778) are also frequently found articulated and preserved in life position.

In one case (Sequence 3; see Fig. 2C), the thoroughly bioturbated pebbly sandstones grade upward into a 70 cm-thick package of gritty sandy siltstones, within which discontinuous 10-20 cm-thick lenses of fine-grained sandstone are intercalated (Fig. 4D). Sandstone beds have sharp bases and display undulatory parallel lamination and oscillation ripple lamination. The foraminiferal assemblage from this package is poor and characterized by the presence of shallow-water benthic genera, including *Ammonia* sp. and *Elphidium* sp. associated with reworked specimens of *Orbulina universa* d'Orbigny, 1839, *Pullenia bulloides* (d'Orbigny, 1846), *Uvigerina peregrina* Cushman, 1923, and *Paracassidulina neocarinata* (Thalmann, 1950).

The sedimentological features displayed by this facies association, including grain size, pervasive bioturbation, and the scarcity of sedimentary structures, are indicative of deposition in a well oxygenated, low energy, shoreface setting, lying in a slightly more distal position compared to the finely laminated pebbly sandstones of FA-1 (i.e., near the lower limit of fair-weather wave base). In this environment, sediment homogenization is attributed to intense biological reworking by benthic organisms during fair-weather periods. The presence of rare remnants

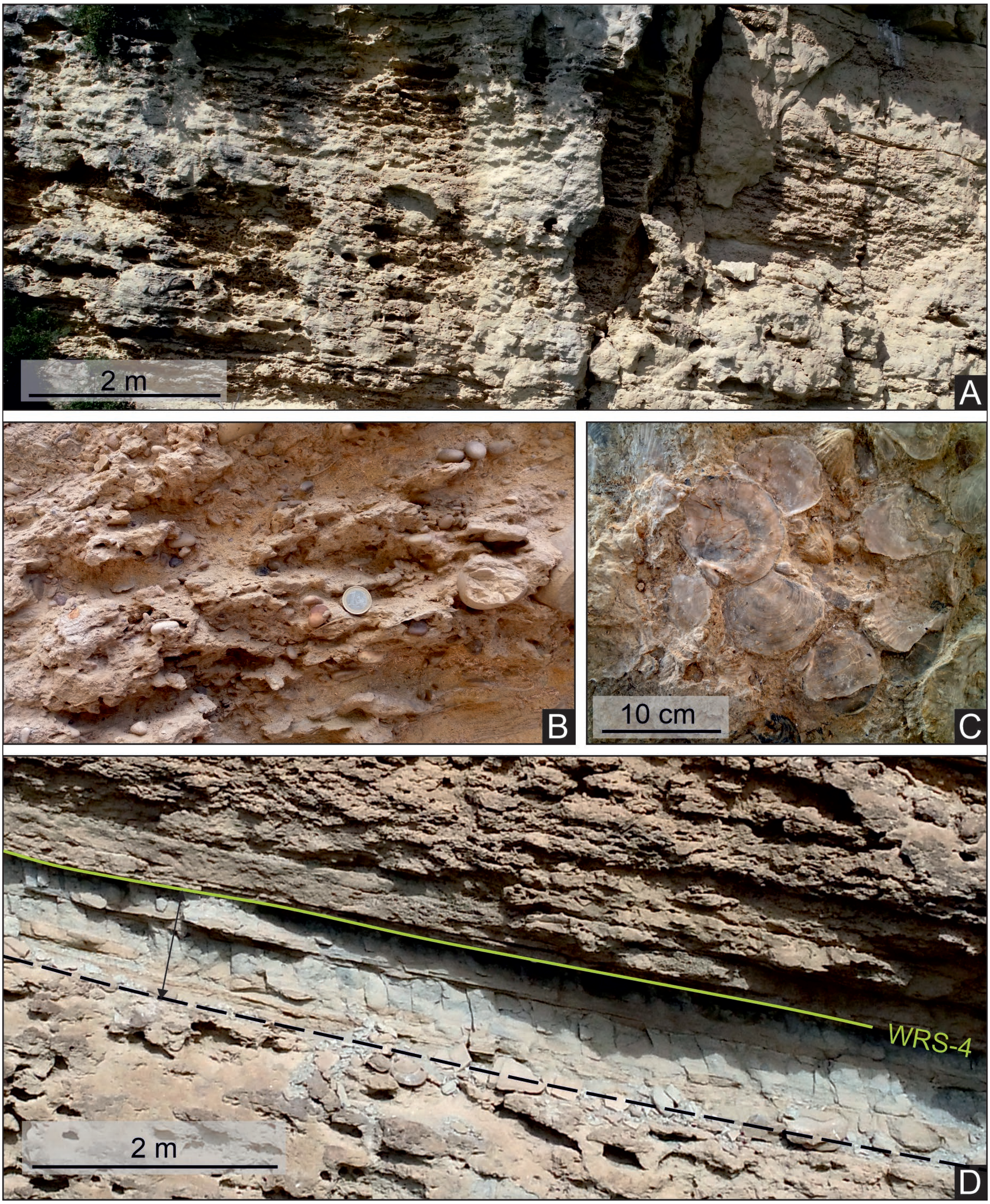

Fig. 4 - Representative sedimentary features of the low-energy lower shoreface deposits associated with FA-2. A) Outcrop overview of the thoroughly burrowed, poorly stratified pebbly sandstones of FA-2. Pervasive bioturbation obscures any trace of remnant physical sedimentary structure, rendering an overall churned fabric to this facies association. B) Close-up view showing well-rounded granule- to pebble-size extrabasinal clasts and shell fragments randomly scattered throughout fine- to coarse-grained sand (coin 23.25 mm in diameter for scale). C) Close-up of bedding plane surface showing flat-lying mollusk valves (mostly pectinids) in pebbly sandstone. D) Photograph showing thoroughly bioturbated pebbly sandstones at base, gradationally overlain (dashed black line) by interbedded blue-gray gritty sandy siltstones and sandstones (arrowed interval), in turn truncated by an abrupt contact (WRS-4) that is overlain by finely laminated pebbly sandstones.

Class	Superfamily	Family	Species	Author	Status
BIVALVIA	Cardioidea	Cardiidae	*Acanthocardia paucicostata*	Sowerby II, 1834	Extant
	Pectinoidea	Pectinidae	*Aequipecten opercularis*	Linnaeus, 1758	Extant
	Arcoidea	Arcidae	*Anadara gibbosa*	Reeve, 1844	Extant
	Pinnoidea	Pinnidae	*Atrina fragilis*	Pennant, 1778	Extant
	Arcoidea	Arcidae	*Barbatia mytiloides*	Brocchi, 1814	Extinct
	Veneroidea	Veneridae	*Callista chione*	Linnaeus, 1758	Extant
	Veneroidea	Veneridae	*Callista italica*	Defrance, 1818	Extinct
	Chamoidea	Chamidae	*Chama gryphoides*	Linnaeus, 1758	Extant
	Veneroidea	Veneridae	*Chamelea gallina*	Linnaeus, 1758	Extant
	Veneroidea	Veneridae	*Circomphalus foliaceolamellosus*	Dillwyn, 1817	Extinct
	Pectinoidea	Pectinidae	*Costellamussiopecten cristatus*	Bronn, 1827	Extinct
	Veneroidea	Veneridae	*Dosinia lupinus*	Linnaeus, 1758	Extant
	Glossoidea	Glossidae	*Glossus humanus*	Linnaeus, 1758	Extant
	Arcoidea	Glycymerididae	*Glycymeris nummaria*	Linnaeus, 1758	Extant
	Pectinoidea	Pectinidae	*Lissochlamys excisa*	Bronn, 1831	Extinct
	Pectinoidea	Pectinidae	*Lissochlamys exotica*	Holten, 1802	Extant
	Limoidea	Limidae	*Limaria hians*	Gmelin, 1791	Extant
	Mactroidea	Mactridae	*Lutraria magna*	da Costa, 1778	Extant
	Mactroidea	Mactridae	*Lutraria* sp.	Lamarck, 1799	
	Tellinoidea	Tellinidae	*Macomopsis cumana*	O.G. Costa, 1830	Extant
	Pectinoidea	Pectinidae	*Manupecten pesfelis*	Linnaeus, 1758	Extant
	Mytiloidea	Mytilidae	*Modiolus adriaticus*	Lamarck, 1819	Extant
	Mytiloidea	Mytilidae	*Modiolus intermedius*	Foresti, 1874	Extinct
	Mytiloidea	Mytilidae	*Mytilus* sp.	Linnaeus, 1758	
	Ostreoidea	Ostreidae	*Ostrea edulis*	Linnaeus, 1758	Extant
	Hiatelloidea	Hiatellidae	*Panopea glycimeris*	Born, 1778	Extant
	Pectinoidea	Pectinidae	*Pecten flabelliformis*	Borson, 1825	Extinct
	Pectinoidea	Pectinidae	*Pecten jacobaeus*	Linnaeus, 1758	Extant
	Veneroidea	Veneridae	*Pelecyora brocchii*	Deshayes, 1836	Extinct
	Veneroidea	Veneridae	*Polititapes vetulus*	Basterot, 1825	Extinct
	Cardioidea	Cardiidae	*Procardium diluvianum*	Lamarck, 1819	Extinct
	Cardioidea	Cardiidae	*Procardium indicum*	Lamarck, 1819	Extant
	Mactroidea	Mactridae	*Spisula subtruncata*	da Costa, 1778	Extant
	Myoidea	Corbulidae	*Varicorbula gibba*	Olivi, 1792	Extant
	Veneroidea	Veneridae	*Venerupis corrugata*	Gmelin, 1791	Extant
	Veneroidea	Veneridae	*Venus nux*	Gmelin, 1791	Extant
GASTROPODA	Architectonicoidea	Architectonicidae	*Architectonica* sp.	Röding, 1798	
	Stromboidea	Xenophoridae	*Aspidophoreas infundibulum*	Brocchi, 1814	Extinct
	Neogastropoda incertae sedis	Cancellariidae	*Bivetiella cancellata*	Linnaeus, 1767	Extant
	Naticoidea	Naticidae	*Cochlis raropunctata*	Sasso, 1827	Extinct
	Conoidea	Conidae	*Conus* sp.	Linnaeus, 1758	
	Cypraeoidea	Cypraeidae	*Cypraea* sp.	Linnaeus, 1758	
	Buccinoidea	Nassariidae	*Demoulia conglobata*	Brocchi, 1814	Extinct
	Epitonioidea	Epitoniidae	*Eglisia spirata*	Sowerby I, 1825	Extant
	Epitonioidea	Epitoniidae	*Epitonium* sp.	Röding, 1798	
	Cerithioidea	Turritellidae	*Helminthia vermicularis*	Brocchi, 1814	Extant
	Tonnoidea	Tonnidae	*Malea orbiculata*	Brocchi, 1814	Extinct
	Naticoidea	Naticidae	*Neverita olla*	De Serres, 1829	Extinct
	Cerithioidea	Turritellidae	*Oligodia spirata*	Brocchi, 1814	Extinct
	Vermetoidea	Vermetidae	*Petaloconchus glomeratus*	Linnaeus, 1758	Extant
	Philinoidea	Scaphandridae	*Scaphander lignarius*	Linnaeus, 1758	Extant
	Tonnoidea	Cassidae	*Semicassis saburon*	Bruguière, 1792	Extant
	Naticoidea	Naticidae	*Sinum striatum*	de Serres, 1829	Extinct
	Neogastropoda incertae sedis	Cancellariidae	*Solatia piscatoria*	Gmelin, 1791	Extant
	Buccinoidea	Nassariidae	*Tritia mutabilis*	Linnaeus, 1758	Extant
	Cerithioidea	Turritellidae	*Turritella tornata*	Brocchi, 1814	Extinct
	Cerithioidea	Turritellidae	*Turritellinella tricarinata*	Brocchi, 1814	Extant
RHYNCHONELLATA	Terebratuloidea	Terebratulidae	*Terebratula ampulla*	Brocchi, 1814	Extinct
THECOSTRACA	Balanoidea	Balanidae	*Balanus* sp.	Costa, 1778	
	Balanoidea	Balanidae	*Concavus concavus*	Bronn, 1831	Extinct
ECHINOIDEA	Spatangoidea	Schizasteridae	*Schizaster* sp.	Agassiz, 1835	

Tab. 1 - Summary table of the invertebrate taxa in the FA-2 of the Spungone Sandstone. The taxonomic nomenclature of taxa relies on WoRMS (2026).

of planar laminae and scattered granules and pebbles, which were likely carried from the foreshore and upper shoreface during storms, clearly indicates the episodic influence of storm-generated waves and currents on sediment deposition. Storms were likely sporadic, moderate-energy events that did not deposit beds thick enough to prevent their subsequent complete reworking by infaunal organisms. The presence of monospecific to low-diversity shell concentrations composed of disarticulated valves and forming laterally extensive beds up to decimetric thickness is interpreted as the result of episodic high-energy hydrodynamic events, most likely storm-generated flows capable of winnowing, transporting, and concentrating bioclastic material, superimposed on an otherwise relatively stable shallow-marine setting (Cau et al. 2019). In this context, FA-2 is interpreted as recording lower shoreface sedimentation under fair-weather conditions, only occasionally affected by storm activity. This interpretation is supported by the composition of the molluscan assemblage, which shows an infralittoral to circalittoral affinity (i.e., Dominici & Forli 2021; Pavia et al. 2022) and documents a highly productive and ecologically complex shallow-marine ecosystem developed under warm-temperate climatic conditions (Mondanaro et al. 2024), characterized by a sandy substrate, and episodic storm-driven disturbance (see Appendix 1).

By contrast, the gritty sandy mudstone is interpreted to reflect deposition at or just below fair-weather wave base, an assertion supported by the deposits

Fig. 5 - Representative sedimentary features of the high-energy lower shoreface deposits associated with FA-3. The rhythmic hummocky cross-stratification consists of sandstone couplets in which cemented sandstone beds, weathering in positive relief, are gradationally overlain by recessive silty sandstones. The basal contact of each cemented sandstone bed with the underlying silty sandstone is typically sharp, thereby defining the base of each successive couplet. Burrowing is largely non-existent or unrecognizable in this facies association.

of predominantly muddy sediments that record accumulation below fair-weather wave base. The intercalated thin sandstone beds that have low-angle undulatory parallel-laminations are interpreted as hummocky cross-stratification generated during infrequent, low-energy storm events.

Rhythmic silty sandstones (FA-3 – strongly storm-dominated lower shoreface): This facies association forms sedimentary packages ranging from 5 to 17 m in thickness, and their tops are always abruptly truncated by transgressive middle shoreface deposits (FA-1). A repetitive succession of alternating well-cemented and poorly-cemented, fine-grained sandstone layers is characteristic of FA-3, with each couplet resting on a sharp, undulating erosional surface that typically exhibits wavelengths of 1 to 5 m. In weathered outcrops, the undulatory surface is directly overlain by a cemented unit that forms a slight positive relief and, across a less distinct boundary, gradually grades upward into a less cemented, more recessive unit (Fig. 5). Internal lamination is not visible, and sandstones show little or no bioturbation (BI = 0-2). The difference in cementation is a diagenetic character, but one reflecting primary textural variations within the sediments. In the cemented intervals, the sand is clean and well-sorted, and with fine-grained material being absent from the interstices, pore spaces are partly or completely filled by chemically precipitated carbonate cement formed during diagenesis and lithification. In contrast, the sands in softer intervals are less well-sorted and contain silt particles mixed with the sand. This silt reduces the available pore space, precluding precipitation of a later cement. FA-3 is present primarily in the upper portion of the Spungone Sandstone, where it reaches a thickness of up to 20 m close to the top of the cliff.

This regular alternation of more strongly and more weakly cemented fine-grained sandstone layers was defined as "rhythmic hummocky stratification"

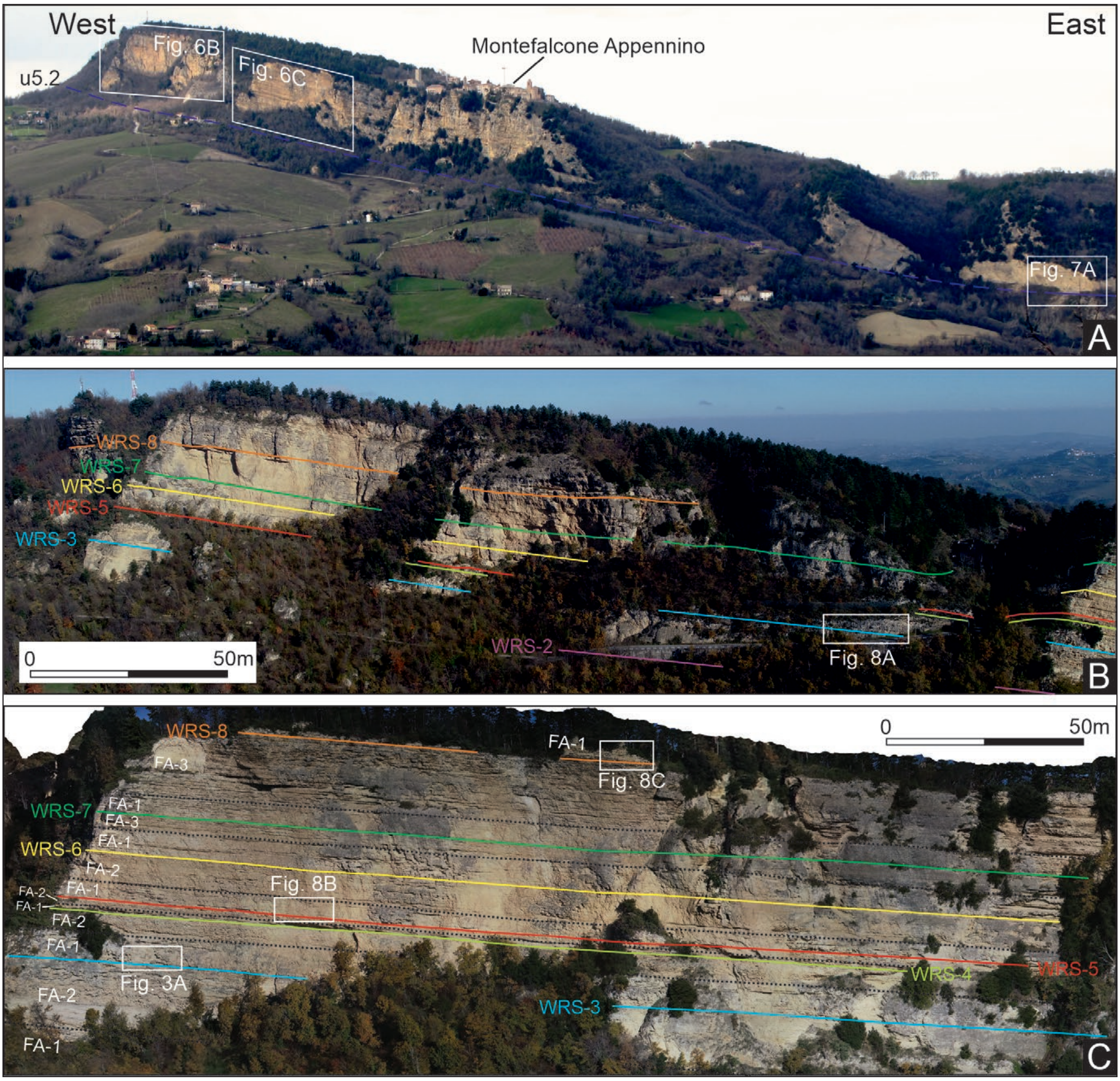

Fig. 6 - Low-angle internal ravinement surfaces partition the Spungone Sandstone into a series of deepening upward sequences. The uppermost part of sequence 8 is not exposed and is assumed to transition into hemipelagic mudstones of the offshore Argille Azzurre Formation. Color codes for the surfaces are given in Fig. 2B. The dashed white lines denote the boundaries between facies associations. A) North-directed oblique, aerial view of the Montefalcone escarpment with position of photos in B, C, and Figure 7A. B) and C) Annotated aerial views showing facies associations and key stratal surfaces.

by Ricci Lucchi (1995), and it has been interpreted as vertical grading recording a high-energy depositional event. The basal scour and the overlying sandstone-silty sandstone couplet are interpreted as the result of individual depositional events that represent the waxing stage of storm encroachment followed by a progressive decline in hydrodynamic energy, and then a return to fair-weather conditions. The rhythmic alternation of more cemented and less cemented intervals is therefore interpreted as the sedimentary expression of repeated storm-generated events, with each sandstone couplet likely recording deposition during storm-peak and subsequent waning-stage conditions (Ricci Lucchi 1995). As storms waned, suspended silt and associated fine-grained sediment progressively settled out and infiltrated the tractional laminae.

Since its first description by Harms et al. (1975), hummocky cross-stratification has been widely interpreted as the product of combined-flow conditions associated with storm events, and thus it is considered a diagnostic sedimentary structure of surface storm activity (Kreisa 1981; Dott & Bourgeois 1982). These conditions are consistent with deposition just above the fair-weather wave base (i.e., the lower shoreface) and involve the interaction between oscillatory wave motion and unidirectional currents (Myrow & Southard 1991). The general absence of burrows produced by deposit-feeding organisms suggests high storm intensity and/or frequency, with repeated storm-wave erosion either inhibiting the development of fair-weather trace fossil assemblages or severely limiting their preservation in this high-energy environment. As such, these sandstone beds represent superimposed storm deposits and are suggestive of more severe storm conditions than FA-2 deposits.

Sequence stratigraphic interpretation

High-frequency sequences composed of mixed siliciclastic-carbonate deposits show a highly variable stratigraphic architecture, characterized by vertical alternations and lateral transitions between carbonate and siliciclastic facies. Compared with purely clastic sequences, mixed systems preserve a similar clastic stratal architecture, although carbonate production and hydrodynamic processes may further influence the geometry and distribution of sediment packages (Nalin & Massari 2009; Zecchin & Catuneanu 2017).

The continuous outcrop exposure along the vertical cliffs bordering the Montefalcone Appennino village allows for direct observations of stratal patterns and stratigraphic architecture within the studied unit. The following section describes general characteristics of the Spungone Sandstone high-frequency sequences and the criteria that define them as discrete chronostratigraphic units. The range of thicknesses observed in these sequences, together with their relative completeness, likely reflects a complex interplay of variations in tectonic subsidence, the magnitude of eustatic sea-level fluctuations, and possibly sediment supply.

Definition of significant bounding surfaces: A set of laterally extensive, unweathered erosional discontinuities, designated WRS-1 through WRS-8 from oldest to youngest, punctuates the Spungone Sandstone and forms the basis for our sequence stratigraphic analysis (Fig. 6). These stratigraphic surfaces subdivide the sediment wedge into a stack of vertically arranged, deepening-upward facies successions and are essentially planar, with barely perceptible relief of up to a few decimeters. They are typified by the unconformable superposition of the middle shoreface facies association (FA-1) on lower shoreface facies associations (FA-2 or FA-3), a relationship reflecting abrupt seaward shifts in facies (i.e., shallowing in formative water depth). The unconformable nature of these surfaces is inferred mainly from: i) abrupt truncation of underlying strata; ii) low-angle onlap stratal terminations; iii) transgressive pebbly lags and/or condensed onlap shellbeds indicating stratal attenuation; iv) abrupt upward shallowing in formative water depth; and v) substrate-controlled *Glossifungites* Ichnofacies (Fig. 7 and Fig. 8), which indicate an erosional origin and provide consistent clues to the presence of stratigraphic hiatuses. As such, these discontinuity surfaces conform to the conventional physical stratigraphic criteria for the recognition of a sequence boundary (e.g., Zecchin & Catuneanu 2013; Neal et al. 2016; Zecchin et al. 2025b, and references therein). Accordingly, they are interpreted as wave-ravinement surfaces (WRS-1 to WRS-8; Fig. 2), formed by wave erosion during the landward passage of a transgressive sea, as described by Swift (1968), Demarest & Kraft (1987), Nummedal & Swift (1987), Cattaneo & Steel (2003), and Zecchin et al. (2019).

Only three of the eight sequence-bounding erosion surfaces noted in the cliff exposures of the Spungone Sandstone are overlain by a transgressive conglomerate lag (WRS-1, WRS-3, and WRS-5 in Figs. 2 and 6) and only one is demarcated by a well-defined *Glossifungites* Ichnofacies (WRS-1). The stratigraphically lowest WRS-1 surface is a regional, low-order angular unconformity (u5.2 in Figs. 2 and 7A) representing where the Spungone Sandstone onlaps the upper Messinian mud-rich strata of the underlying substrate (Fig. 7). This surface differs from succeeding ones by being overlain by mud rip-up clasts and shell debris embedded in a matrix of sand and mud, and by being demarcated by densely crowded, sharp-walled burrows dominated by *Thalassinoides* and spiraled *Gyrolithes* traces recording an ichnological omission suite. The rip-up mud clasts are well-rounded and were reworked directly from the stratigraphically subjacent Messinian strata to form a transgressive lag, whereas the coarse-grained, shell-rich basal facies is interpreted as a transgressive hiatal concentration developed at the base of a transgressive sand sheet during a period of slow net sedimentation (onlap shellbed sensu Kidwell 1991, 1993; Abbott 1998; Kondo et al. 1998). As such, the transgressive lag and the onlap shellbed overlying WRS-1 is interpreted to result from a combination of substrate reworking and condensation due to storm waves and currents, which lead to sediment bypassing and winnowing of fines during shoreface retreat (i.e., Cattaneo & Steel 2003; Zecchin et al. 2024 and references therein). The passive filling of the traces with shell-rich material derived from the overlying onlap shellbed indicates the firm or stiff character of the substrate at the time of the colonization, which was the result of a previous subaerial exposure and/or exhumation by ravinement (MacEachern & Pemberton 1992; Pemberton & MacEachern 1995; Ghibaudo et al. 1996; MacEachern et al. 2012).

The architecture of the stratigraphic sequences: Facies associations recur vertically in consistent and predictable stratigraphic patterns and combine to define a succession of eight stratal units displaying a deepening-upward progression, from middle to lower shoreface, inferred to reflect base-level rise and transgression. Following Zecchin & Catuneanu (2013) and Catuneanu & Zecchin (2013), each of these stratal units is regarded as a high-frequency depositional sequence, with thicknesses ranging from about 4 to 25 m.

A major challenge in high-resolution, outcrop-based sequence-stratigraphic analysis of fully shoreface successions is the recognition of the maximum flooding surface and the consequent distinction between transgressive and highstand systems tract deposits. In such settings, the maximum flooding surface commonly lacks a clear expression in the facies architecture, rarely coincides with a distinct facies contact, and is therefore regarded as a cryptic stratigraphic horizon (Zecchin et al., 2023). Recently, Zecchin et al. (2021) demonstrated that its stratigraphic position can be constrained through an integrated sedimentological and micropaleontological approach, combining variations in benthic foraminiferal abundance, diversity, fragmentation, and ecological composition. This approach, however, cannot be applied to the Spungone Sandstone because its strongly cemented shoreface deposits prevent the recovery of sufficiently well-preserved micropaleontological assemblages suitable for quantitative analysis. Consequently, the internal architecture of the high-frequency depositional sequences was reconstructed exclusively from sedimentological evidence, using facies analysis and the vertical stacking and lateral relationships of facies associations rather than independent micropaleontological constraints. Accordingly, these sequences are interpreted as top-truncated and incomplete in terms of systems tracts, as they consist exclusively of transgressively stacked facies associations. The surface of subaerial exposure (i.e., the sequence boundary sensu stricto), together with the highstand and the falling-stage systems tracts of the underlying sequence, was systematically removed by erosion during landward shoreline migration. In this context, ravinement surfaces represent effective pathways for sediment bypass across the inner shelf and ultimate distribution in the deeper-water basin sink.

Based on the characteristic vertical succession of facies associations, two basic sequence motifs have been recognized, termed *WSA* and *SSD*, representing shoreface deposition during a cycle of relative sea-level change under weakly storm-af-

Fig. 7. A) Panoramic view of the basal (angular) unconformity (u5.2). This unconformity places the pale yellow, gently eastward dipping strata of the upper Zanclean Spungone Sandstone over folded, blue-gray mudstones of the upper Messinian Laga Formation (position of this image is provided in Figure 6A). It reflects a major sub-aerial erosional surface colonized by marine organisms during ensuing transgression. The pale blue-gray color of the Spungone sediments directly overlying the unconformity is due to the high degree of mud-size matrix in the basal shell-rich interval. B) The u5.2 unconformity (shown by white arrows) is a *Glossifungites* Ichnofacies-demarked wave-ravinement surface (WRS-1) indicating the stiff nature of the underlying mudstones and a prolonged period of erosion and omission. The substrate-controlled assemblage includes *Gyrolithes* (Gy) and *Thalassinoides* (Th) burrows subtending from the erosional discontinuity and descending up to 60 cm into the subjacent mudstones. Burrows are 2-3 cm in diameter and have been passively filled with coarse shelly and sandy sediment derived from the superjacent shellbed. Overlying the surface is a 20 cm thick lag composed of well-rounded, rip-up mudstone clasts (black arrows), which were plucked out from the underlying succession, and a thoroughly burrowed mixture of shells and highly fragmented skeletal material (onlap shellbed) set in a matrix of sand and mud. C) Blow-up of a *Gyrolithes* burrow displaying a vertical to subvertical coiling axis. The trace is preferentially cemented and weathers out in relief of muddy host sediment forming a spiral-shaped burrow cast. Coin is 2.42 cm in diameter. D) Blow-up of an irregularly inclined *Thalassinoides* burrow. Hammer head is 17 cm long.

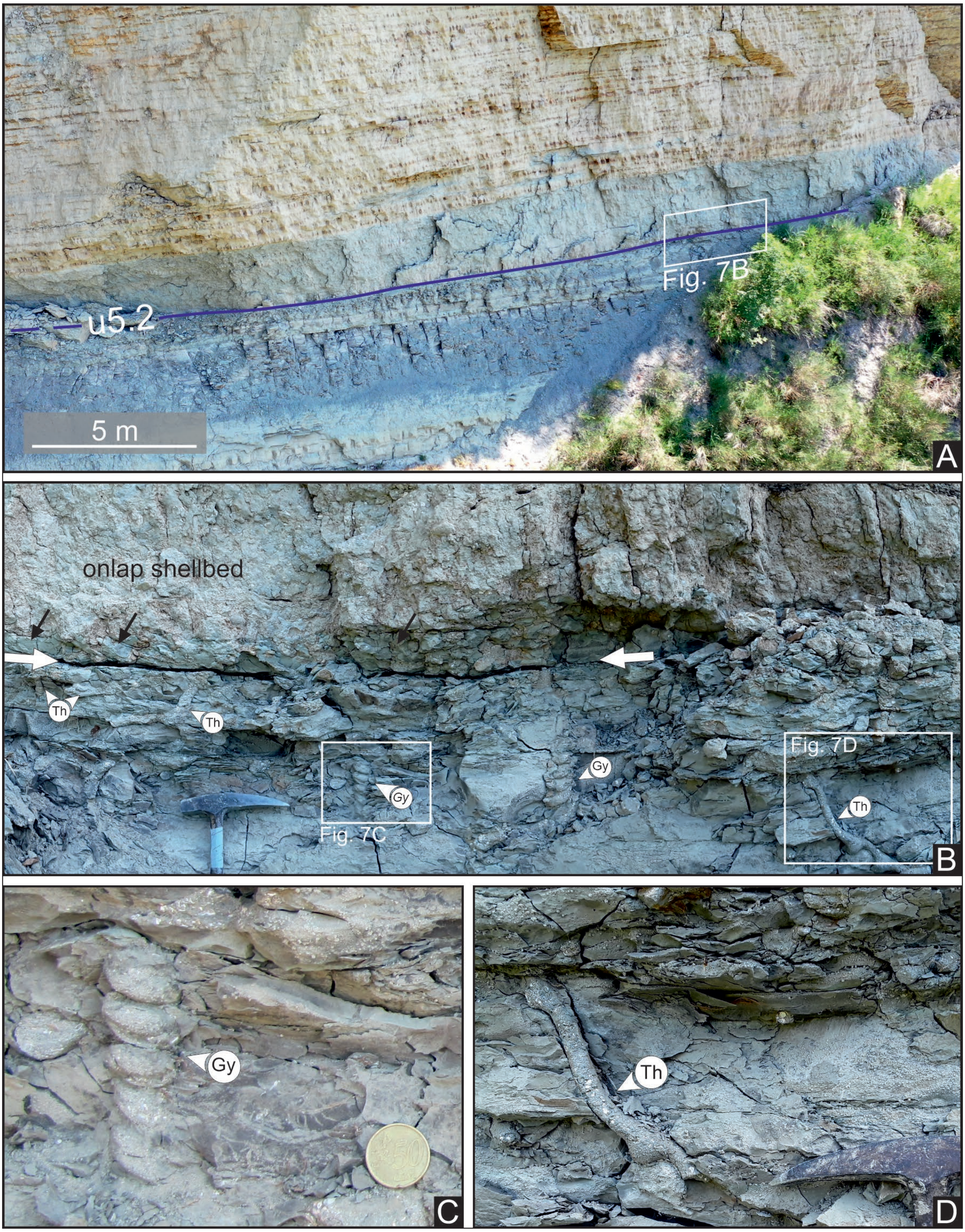
u5.2
Fig. 7B
5 m
A
onlap shellbed
Th
Th
Gy
Gy
Fig. 7C
Fig. 7D
Th
B
Gy
C
Th
D

Fig. 7

fected and strongly storm-dominated conditions, respectively. Motif *WSA* characterizes the lower five sequences and represents the most common facies succession. It begins with the middle-shoreface FA-1 facies association that is overlain by the lower shoreface FA-2 facies association. Motif *SSD* occurs in the upper three sequences and is broadly similar to *WSA*, but the middle-shoreface FA-1 facies association passes gradationally upward into the lower shoreface FA-3 facies association.

Sandstone composition

To characterize the detrital modes of the Spungone Sandstone, a total of sixteen fine- to medium-grained sandstone samples were collected along the stratigraphic section measured at Montefalcone Appennino (see Fig. 2B for sample locations). These samples were analyzed through petrographic thin-section analysis and point counting of seven of those sixteen samples, complemented by XRD and SEM investigations.

X-Ray Diffraction analyses

XRD analyses of powdered samples provided semi-quantitative information on the relative abundances of calcite, quartz, feldspars, and muscovite (Fig. 9). The dominant mineralogical phases identified in the analyzed samples are calcite ($CaCO_3$) and quartz (SiO_2), corresponding to the two most intense diffraction peaks. All diffractograms also consistently show the presence of feldspars sensu lato and muscovite. Additional minor peaks can be attributed to other mineral phases occurring in minor to trace amounts. A closer inspection of the most intense diffraction peaks of calcite (d = 3.03 Å) and quartz (d = 3.34 Å) reveals substantial variability in their relative intensities among the samples. Comparison of these peak intensities allows estimation of the relative abundance of calcite and quartz, expressed as Cal/(Cal + Qtz) in wt.%. Based on these, calcite contents range from 48 to 86 wt.% in samples from FA-1, from 60 to 75 wt.% in FA-2 samples, and from 76 to 78 wt.% in the two samples from FA-3.

Calcite in the analyzed samples may derive from multiple sources, including clastic calcite grains, microfossils, skeletal fragments of marine macrofossils (especially bivalves and gastropods), limestone lithic fragments, and pore-filling cement. The calcite content determined by XRD represents the total calcite fraction, and the technique does not allow to discriminate among the different textural or genetic forms of calcite occurring in the samples.

Petrographic analysis and detrital modes of the sand fraction

The seven sand samples all plot in the lithic arenite field (Fig. 10), with the majority of grains being angular to subrounded in shape, and primarily in the size range 88 - 250µm (vfU – fU sized sand, Fig. 10). The angular to subangular shape of most non-carbonate framework grains as well as many carbonate grains is evident (Figs. 10, 11), as is the variety of bioclasts and micrite framework grains. The presence of glauconite and of an abundant and diverse bioclast assemblage is evidence that this sand has a distinct marine affinity. Ferroan and non-ferroan carbonate minerals are present, both as framework grains and as interparticle cement (Figs. 10, 11). Furthermore, there are varying degrees of intensity in the color of the stain taken by the ferroan calcite, which ranges from mauve to lavender

Fig. 8 - Example of wave-ravinement surfaces (WRS) separating high-frequency sequences in the Spungone Sandstone (positions of images provided in Figure 6B and C). These erosional discontinuities are polygenetic unconformities originated from subaerial erosion during times of relative sea-level lowering and subsequent reworking by the erosive shoreface during the ensuing transgression. Each surface rests directly on the truncated transgressive systems tract of the underlying sequence and marks an abrupt basinward offset of facies, so that shallower-water deposits rest on deeper deposits. Yellow lines denote landward onlap terminations of sandstone beds on the basal unconformity. A) WRS-3 rests upon weakly storm-affected lower shoreface deposits and is overlain by middle shoreface deposits, recording a minor basinward offset facies. It is not associated with a lag or condensed onlap shellbed. Road sign approximately 2 m tall. B) UAV image of inaccessible cliff exposure. WRS-5 overlies weakly storm-affected lower shoreface deposits and is mantled by a middle shoreface, closely-packed lag of well-rounded lithic pebbles (and rare cobbles) up to 30 cm thick, recording a minor basinward offset of facies. This lag is strictly related to the formation of the ravinement surface and is regarded as resulting from the accumulation of pebbles that were excavated from the subjacent gravel-bearing sandy deposits and redistributed during coastal retreat, while the fine sediments were winnowed into suspension and transported offshore. C) UAV image of inaccessible cliff exposure. WRS-8 is interpreted as the final wave-ravinement surface within the Spungone Sandstone. It overlies strongly storm-dominated lower shoreface deposits and is overlain by upper shoreface pebbly sandstones, recording a minor basinward dislocation of facies. This surface is not associated with a lag or condensed onlap shellbed.

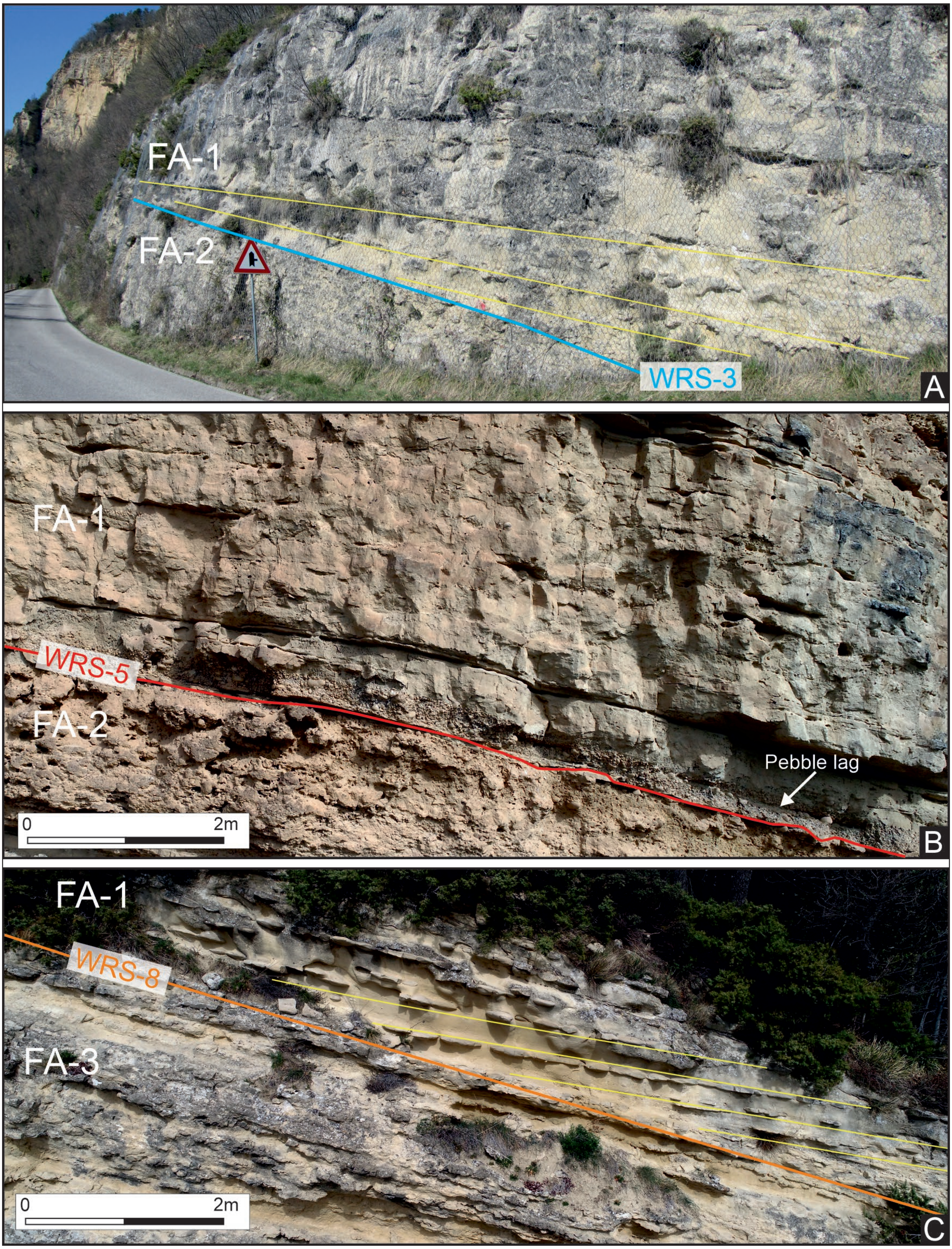

Fig. 8

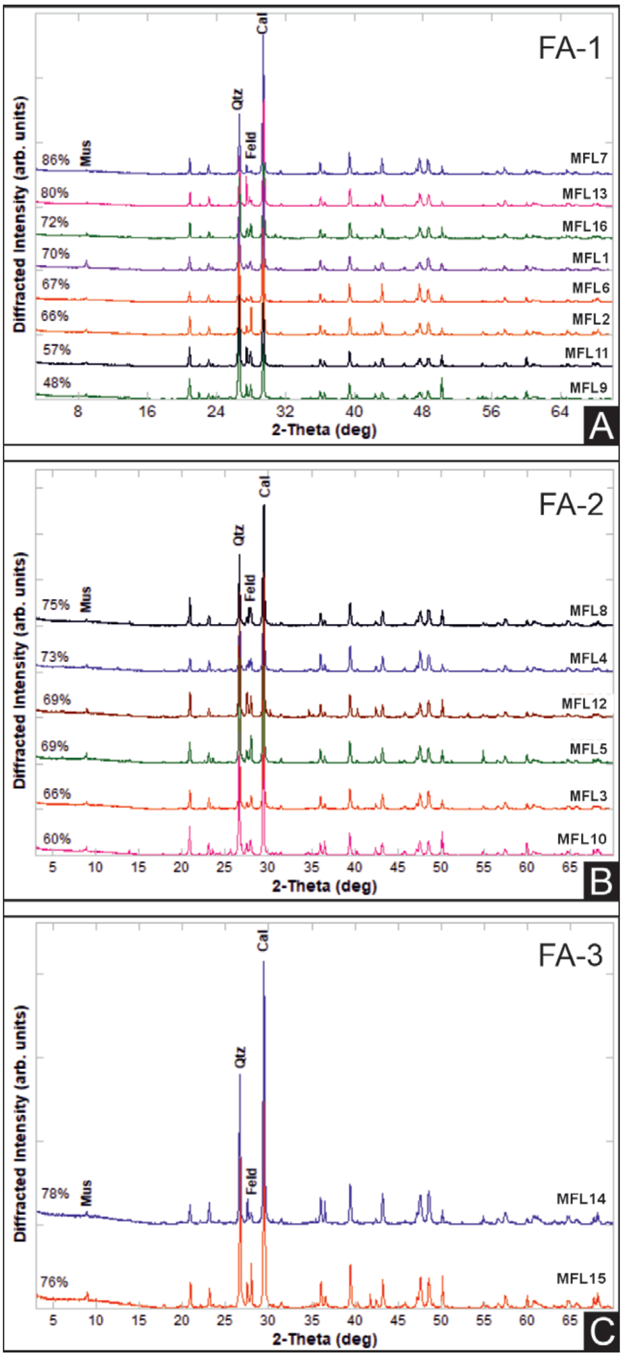

Fig. 9 - Powder X-ray diffraction patterns of (A) FA-1, (B) FA-2, and (C) FA-3. The vertical axis shows the diffracted intensity of each sample (arbitrary units), while the horizontal axis represents the 2-theta diffraction angle. Sample labels are indicated on the right side of each pattern, whereas the calculated Cal/(Cal + Qtz) ratio (wt%) is reported on the left side of each spectrum. The most intense peaks of the main phases are labeled as Cal (calcite), Qtz (quartz), Feld (feldspars, sensu lato), and Mus (muscovite).

to purple to an intense royal blue (Fig. 10), which reflects the variation in iron content; the more intense the blue coloration, the higher the ferrous iron content (Hitzman 1999).

Framework grains: The principal framework grain population is comprised of abundant angular to subrounded quartz and a variety of lithic fragments including many extrabasinal carbonate grains (Figs. 10, 11). Point-counting results form the basis for the ternary diagrams in Figure 12, showing the abundances of framework grains, excluding bioclasts.

Quartz is present as monocrystalline (common, or plutonic), macro polycrystalline (both stretched and unstretched, unstretched >> stretched), and micro to crypto polycrystalline (chert) grains (Fig. 11A-D). A single detrital grain of zebraic chalcedony was observed. Schistose metamorphic quartz occurs in trace amounts (Fig. 11E, F), and although it is predominantly polycrystalline quartz, those grains are considered metamorphic rock fragments (MRFs) by virtue of the mica in them, which indicates derivation from an eroding schistose source rock. Many if not most of the detrital micas present were probably also sourced by schists.

The abundant carbonate framework grains exhibit appreciable compositional diversity that includes a variety of bioclastic debris (Figs. 10, 11D, G, H), and different textural characteristics, such as fossiliferous and unfossiliferous wackestones, packstones, and grainstones. Sedimentary rock fragments (SRFs) and angular to rounded micritic SRFs also occur (Figs. 10, 11C, E, G, H). Nearly all the carbonate SRFs are considered to be of extrabasinal origin on account of their being thoroughly admixed with the detrital aluminosilicate framework grains, but the framework grains of rounded micritic SRFs in these sands warrant special mention. Because carbonate framework grains are almost always sedimentary particles of intrabasinal origin, and because detrital mode analysis of sandstones is focused on extrabasinal sediments and their provenance, it is customary to exclude the common carbonate allochems (ooids, intraclasts, bioclasts, peloids) from point counts of framework grains. In the sand fraction of the Spungone Sandstone, a possible exception to this general rule needs to be noted, specifically the likelihood that some of the micritic SRFs (Figs. 10, 11C, G, H) may actually be peloids rather than reworked sand-sized grains of micrite that were weathered from disintegrating lime mudstones in the source terrane and then transported to the site of deposition. As the distinction is rare-

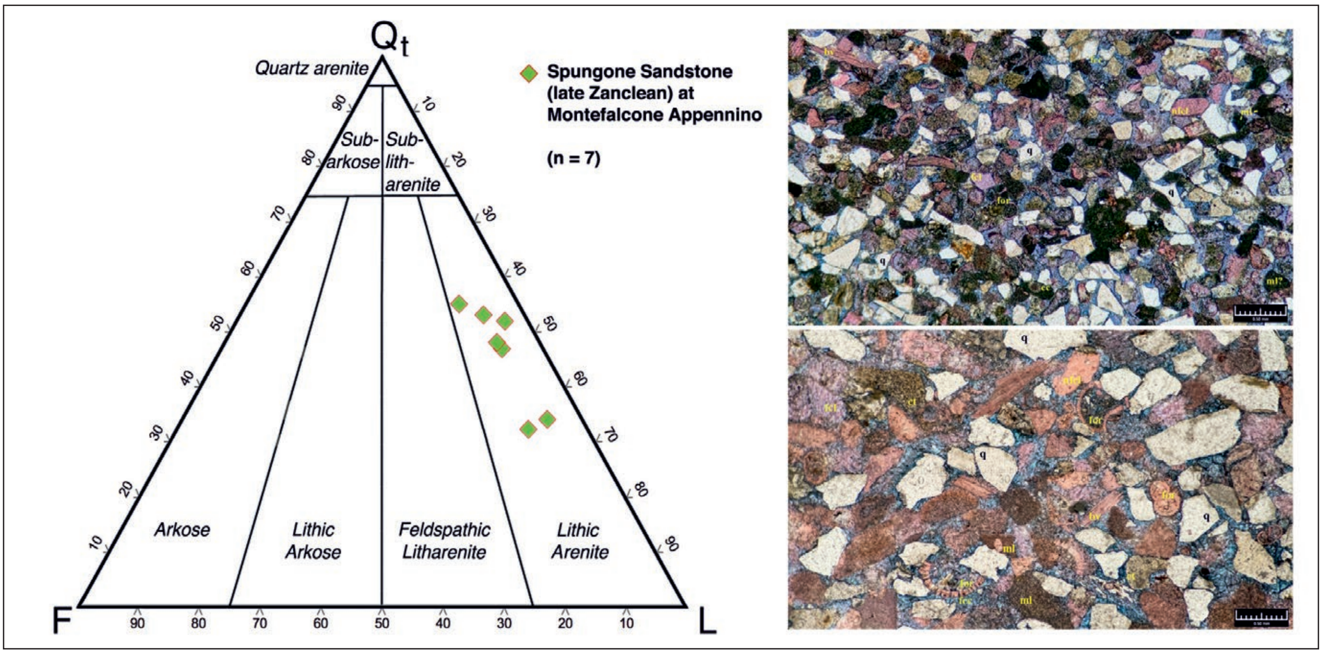

Fig. 10 - At left: ternary QFL diagram (modified after Folk et al. 1970; Folk 1980) used to determine compositions of the Spungone Sandstone samples; all are lithic arenites, with 30-55% quartz, 35-60% lithics, and 5-10% feldspar, as the framework grain populations. The Q pole is shown as Qt, total quartz including polycrystalline grains. At right: photomicrographs showing the typical appearance of the Spungone Sandstone (lower is MFL4; upper is MFL15) in thin sections stained for carbonate minerals with the standard Dickson (1965) method; both are in plane polarized light (PPL). Abbreviations for framework grains and cements: bv-bivalve, ct-chert, ec-echinoderm, fcc-ferroan calcite cement, fcl-ferroan calcite lithic grain, for-foraminifera, ml-micritic lithic grain, nfcl-non-ferroan calcite lithic grain, q-quartz. The scale bar in the lower right corner is 0.5 mm.

ly straightforward, this issue was addressed, to the extent possible, during point counting by excluding those micrite framework grains that are rounded to well-rounded, because those are the grains most likely to be actual peloids, and more specifically, to be fecal pellets produced as intrabasinal sedimentary particles by the organisms living in the depositional basin while the sand was accumulating. By contrast, angular to subangular framework grains of micrite are far more likely to be SRFs derived from the weathering and erosion of lime mudstone in the source terrane. Although this adjustment is by no means ideal, it does reduce, at least to some extent, the possibility of overcounting micritic sedimentary particles of intrabasinal origin in the framework grain population.

Feldspar grains, which comprise ≤ 10% of the framework grain population (Figs. 10, 11A, B), include minor twinned plagioclase and untwinned potassium feldspar (probably orthoclase), and a trace amount of microcline and perthite framework grains. Other lithic framework grains present in minor to trace amounts include: 1) muscovite; 2) schistose polycrystalline quartz metamorphic rock fragments (MRFs) that are recognizable by their internal foliation resulting from oriented mica flakes (most commonly muscovite) within the grain; 3) biotite, including many grains that have been chloritized to varying extents; 4) glauconite; 5) dolomite SRFs; and 6) various heavy and/or opaque minerals including zircon, tourmaline, and rutile. No volcanic rock fragments (VRFs) or quartzofeldspathic rock fragments (QFRFs) were observed in any of the seven sandstone samples analyzed (Fig. 12).

Whole and fragmental bioclasts are sparse to common, and include foraminifera, bryozoans, bivalves, echinoderms, and red algae (Figs. 10, 11).

Cements: The principal cement in all samples is ferroan calcite that, based on its royal blue staining, indicates a slightly higher than usual iron content. This contrasts with the ferroan calcite comprising many of the extrabasinal carbonate SRFs, which exhibit a slightly lower iron content (Hitzman 1999), as evidenced by their mauve to lavender staining (Figs. 10, 11). The possibility that this blue stained cement is ferroan dolomite is refuted by the subtle difference in color (royal blue for ferroan calcite, turquoise for ferroan dolomite), and by the lack of dolomite in the diffractograms obtained by XRD analyses. Therefore, non-ferroan calcite is common as both detrital limestone SRFs and calcareous bioclasts, but much less common as a cement, whereas ferroan calcite is present not only as some detrital limestone SRFs, but as the most common cement in these sandstones as well.

Detrital modes: The detrital modes for the Spungone Sandstone are shown in four ternary diagrams (Fig. 12). The fields in the QFL and QmFLt diagrams are after Dickinson et al. (1985), the fields in the QpLvLs diagram are modified after Ingersoll (1983), Dickinson & Suczek (1979, dashed), Dickinson et al. (1983), Ingersoll & Suczek (1979), and Martini et al. 2011, solid), and the fields in the LmLv(Ls+C) diagram are from Ingersoll & Suczek (1979) and Ingersoll (1983) as modified by Zuffa (1987) and Valloni et al. (2002). The sand fraction in the seven samples of the Spungone Sandstone plots in the recycled orogen field of the QFL diagram, and in the transitional recycled field of the QmFLt diagram. We interpret this as a reflection of the overall character of the Mesozoic-Cenozoic Umbria-Marche sedimentary succession, with its abundant cherty limestones, which is the probable source of these sandstones. The QpLvLs and LmLv(Ls+C) diagrams, which help to parse out the detrital modes of the lithic framework grain population by further subdivision into discrete provenance areas, show that the lithic fraction of these sandstones consists almost exclusively of carbonate SRFs and chert. Specifically, the petrographic findings presented here show that the data centroid on the QpLvLs and LmLv(Ls+C) diagrams in Figure 12 is continuing to migrate toward the Ls and Ls + C endpoints respectively, as there are no VRFs, and only very few MRFs in these sands.

Scanning Electron Microscope results

A representative backscattered electron (BSE) image reveals the presence of both euhedral and anhedral grains of small size, predominantly < 100 μm. The most common mineral phases identified include quartz and calcite (occurring as discrete crystals, microfossil or fossil fragments, limestone lithic clasts, and pore-filling cement), as well as feldspar, plagioclase, muscovite, and biotite. Several accessory minerals have also been identified including allanite-(Ce), almandine, fluorapatite, hematite, ilmenite, magnetite, monazite-(Ce), monazite-(La), titanite (sphene), xenotime, and zircon (Fig. 13). All these minerals typically occur as fine-grained particles embedded within the cement or as constituents of lithic fragments. Grain sizes are generally very small (commonly < 50 μm), which may reflect mechanical abrasion associated with long-distance transport.

Zircon grains have been found in all the samples examined (Fig. 14). In most cases, they are small (usually from few μm up to 60 μm) with rare crystals up to 120 μm length. Only one zircon crystal has been found with a length of 200 μm. Zircon grains occur both as anhedral to subhedral grains embedded in carbonate cement, or as part of a lith-

Fig. 11 - Photomicrographs of the Spungone Sandstone showing additional details of framework grains, cements, and textures as observed in thin section. All samples are stained for carbonate minerals as in Fig. 10, and all scale bars are 400 μm. PPL: plane polarized light; XPL: cross polarized light. Framework grain and cement abbreviations are as for Fig. 10, with additional abbreviations as noted below. A) Siliciclastic and carbonate framework grains including a large chert framework grain at center and smaller chert grains scattered about; plagioclase feldspar (pf), stretched polycrystalline quartz (p), and various foraminifera skeletal debris both whole and broken (f) are present. Other framework grains (not labeled) include numerous subrounded to angular monocrystalline quartz (white), and carbonate sedimentary rock fragments (SRFs) that vary compositionally from non-ferroan limestone (pink) to ferroan limestone to dolomitic limestone (lavender to blue). PPL. B) Same as (A); note the various textures in the chert, feldspar, and macrocrystalline quartz framework grains. XPL. C) Siliciclastic and carbonate framework grains including part of a spicular chert pebble at bottom, and muscovite (m), glauconite (g), micrite peloids (p), and various foraminifera bioclasts. PPL. D) A large gastropod in which the primary biomoldic porosity has been completely infilled by sediment, suggesting that the empty shell was tumbled about in the shallow marine environment and then filled in with the surrounding sand. The yellow arrows point to the ferroan sparry calcite cement that is abundant in these sandstones. PPL. E) Large schistose quartz grain at center with foliation defined by muscovite, indicating that this is a metamorphic rock fragment (MRF). PPL. F) Same as (E); note additional framework grains (not labeled) including monocrystalline quartz, plagioclase, peloids, and various bioclasts including foraminifera and bivalve fragments. XPL. G) Mix of framework grains (not labeled) including various foraminifera, peloids, and quartz, with the ferroan calcite cement in this sample being particularly iron-rich as indicated by the blue tint of the stain that contrasts with the pink stained non- ferroan calcite and the lavender stained ferroan calcite that comprise many of the carbonate framework grains in these sandstones. PPL. H) Large bivalve bioclast fragment at right center composed of pink stained non-ferroan calcite and which exhibits prominent prismatic structure typical of many bivalve shells. Other framework grains (not labeled) include various carbonate SRFs, foraminifera fragments, and quartz, all of which are cemented by lavender colored ferroan sparry calcite cement. PPL.

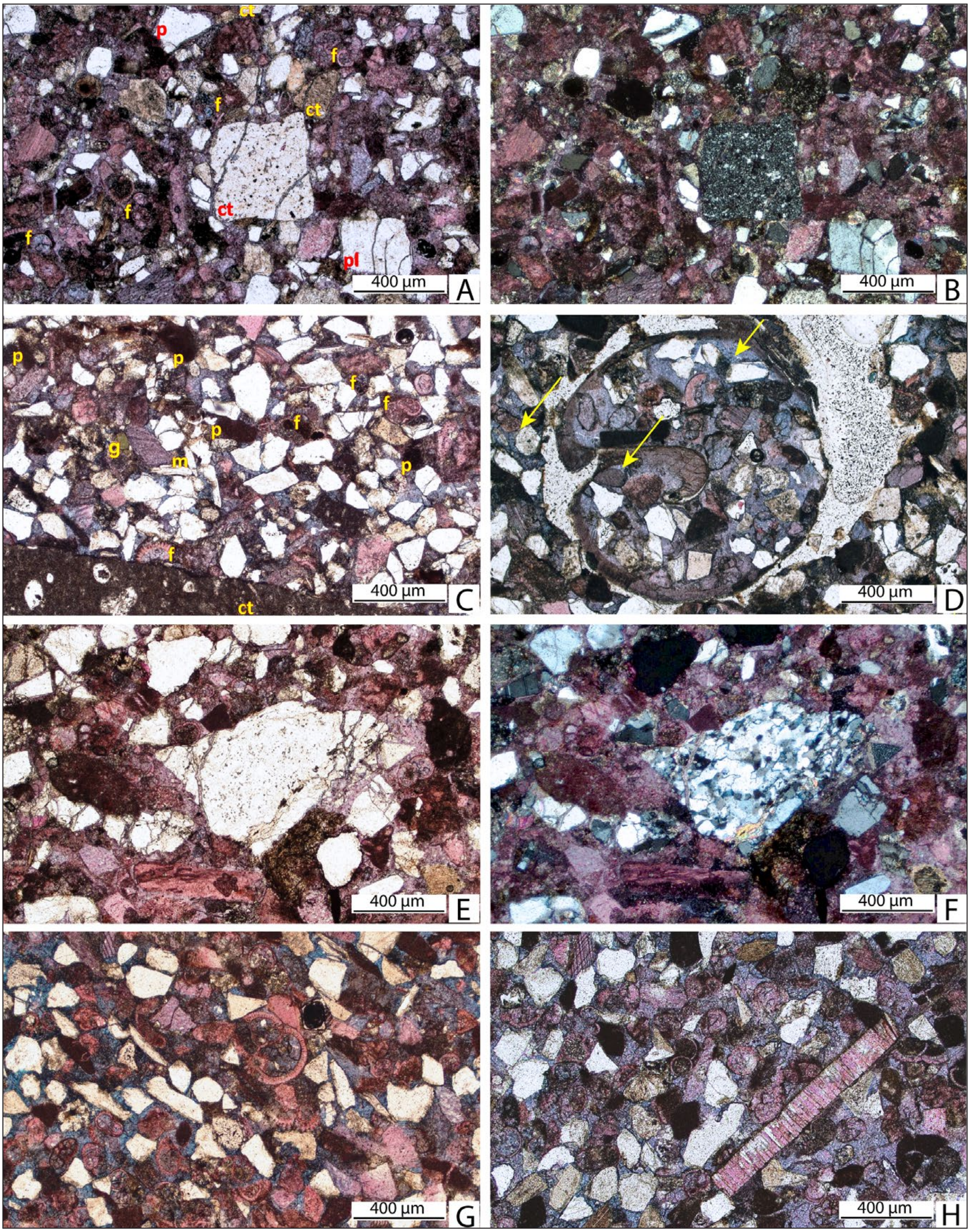

Fig. 11

Detrital modes of samples (300 point counts each)

Sample No.	*Qm*	*Qp*	*Chert*	*Q*	*K*	*P*	*F*	*Lm*	*Ls (C)*	*Ls (M)*	*Other*	*Qp (recalc.)*	*L*	*Lt*	*Ls (recalc.)*	*Ls + C*	*QFL*	*QmFLt*	*QpLvLs*	*LmLv(Ls+C)*
MFL-1	33	14	5	52	3	1	4	1	33	9	1	32	44	63	68	99	$Q_{52}F_4L_{44}$	$Qm_{33}F_4Lt_{63}$	$Qp_{32}Lv_0Ls_{68}$	$Lm_1Lv_0(Ls{+}C)_{99}$
MFL-3	30	15	10	55	6	4	10	2	22	11	0	42	35	60	58	98	$Q_{55}F_{10}L_{35}$	$Qm_{30}F_{10}Lt_{60}$	$Qp_{42}Lv_0Ls_{58}$	$Lm_2Lv_0(Ls{+}C)_{98}$
MFL-4	32	10	5	47	5	2	7	1	25	19	1	26	46	61	74	99	$Q_{47}F_7L_{46}$	$Qm_{32}F_7Lt_{61}$	$Qp_{26}Lv_0Ls_{74}$	$Lm_1Lv_0(Ls{+}C)_{99}$
MFL-6	31	10	7	48	6	1	7	1	25	18	1	28	45	62	72	99	$Q_{48}F_7L_{45}$	$Qm_{31}F_7Lt_{62}$	$Qp_{28}Lv_0Ls_{72}$	$Lm_1Lv_0(Ls{+}C)_{99}$
MFL-8	32	10	11	53	5	2	7	1	22	17	0	34	40	61	66	99	$Q_{53}F_7L_{40}$	$Qm_{32}F_7Lt_{61}$	$Qp_{34}Lv_0Ls_{66}$	$Lm_1Lv_0(Ls{+}C)_{99}$
MFL-14	26	4	4	34	4	2	6	0	33	27	0	11	60	68	89	100	$Q_{34}F_6L_{60}$	$Qm_{26}F_6Lt_{68}$	$Qp_{11}Lv_0Ls_{89}$	$Lm_0Lv_0(Ls{+}C)_{100}$
MFL-15	23	3	6	32	9	1	10	0	30	27	1	14	58	67	86	100	$Q_{32}F_{10}L_{58}$	$Qm_{23}F_{10}Lt_{67}$	$Qp_{14}Lv_0Ls_{86}$	$Lm_0Lv_0(Ls{+}C)_{100}$

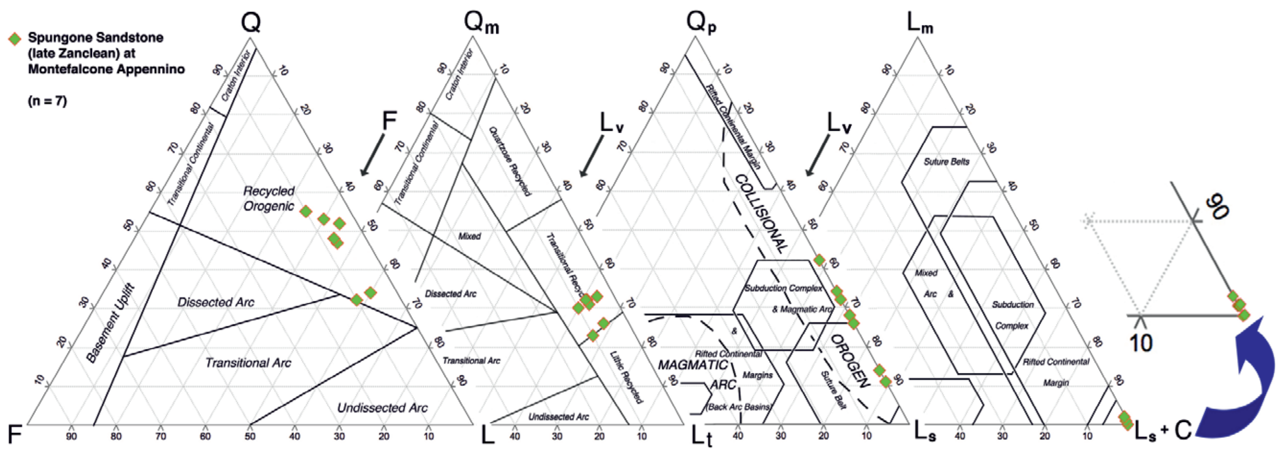

Fig. 12 - Petrographic point-counting data of the Spungone Sandstone. Qm=monocrystalline quartz; Qp=polycrystalline quartz; Chert=chert grain; Q=total quartz, Qm+Qp+Chert; K=K-feldspar; P=plagioclase; F=total feldspar; Lm=total MRFs; Ls(C)=total non-micritic carbonate SRFs; Ls(M)=total micritic carbonate SRFs; Other=accessory minerals (micas, glauconite, heavy minerals); Qp (recalc.)=polycrystalline quartz, recalculated for the QpLvLs mode; L=total lithics; Lt=L+Qp+Chert; Ls (recalc.)=SRFs recalculated for the QpLvLs mode; Ls+C=total SRFs recalculated for the LmLv(Ls+C) mode; Lv=total VRFs including meta-volcanic grains; Ls=total SRFs including meta-sedimentary grains. Last four columns are plotted graphically in the QFL, QmFLt, QpLvLs, and LmLvLs+C ternary diagrams that delineate detrital modes for the sand fraction in the seven samples that were point counted. The overall provenance of these sands based on the QFL and related QmFLt diagrams is a recycled orogenic source with a mix of quartz and lithic grains that skews toward the L/Lt pole. Scrutiny of the lithic grain subpopulations and more precise constraint of their provenance is possible with the QpLvLs, and LmLvLs+C diagrams, which show that metamorphic rock fragments (MRFs) are rare, and volcanic rock fragments (VRFs) are completely lacking in the lithic rock fragment fraction. Collectively, this absence of VRFs and the overall scarcity of MRFs indicates that a collisional orogen is the most likely provenance. This fits with these sands being sourced primarily from weathering and erosion accompanying the unroofing of the Umbria-Marche Mesozoic-Cenozoic cherty limestones, and to a perhaps equal or slightly lesser extent the Messinian turbiditic sandstones of the Laga Formation. Sedimentary rocks of the Umbria-Marche sequence and the Laga Formation are extensively exposed in uplifted areas of the Apennines, a collisional orogen, such as the Sibillini region that is due west of the Montefalcone Appennino section. Arrow (right) points to an inset that shows the magnified details of all 7 samples that are tightly clustered at the Ls+C endpoint of the LmLv(Ls+C) diagram.

ic fragment (in which case it appears as subhedral to euhedral crystals), associated with feldspars, plagioclase, quartz or biotite. A suite of zircon crystals initially identified in thin section with the polarizing microscope and then by SEM, was analyzed further using laser ablation inductively coupled plasma mass spectrometry (LA-ICPMS) to gain additional understanding of their trace element content and ages. All the zircon grains examined display small amounts of hafnium (typically 1 mole % relative to Zr). Although zircon crystals are expected to contain from a few hundred ppm up to ~2000 ppm of total REE, EDS analyses of all the examined crystals did not reveal the presence of detectable REE. Accurate mapping of elemental contents across zircon crystals did not evidence significant compositional zonation. U-Pb geochronologic analyses of three zircon grains by LA-ICPMS yielded crystallization ages of 261, 262, and 675 Ma.

It is noteworthy that, in some cases, heavy minerals, particularly zircon, ilmenite, and titanium oxides (probably rutile), normally present in very low amounts, are concentrated in small areas to form clusters approximately 100-200 μm wide (Fig. 15). This concentration closely resembles the mineral associations found within *Psammophaga zirconia* Sabbatini, Bartolini & Morigi, 2016, a recently described benthic foraminifer that feeds in pres-

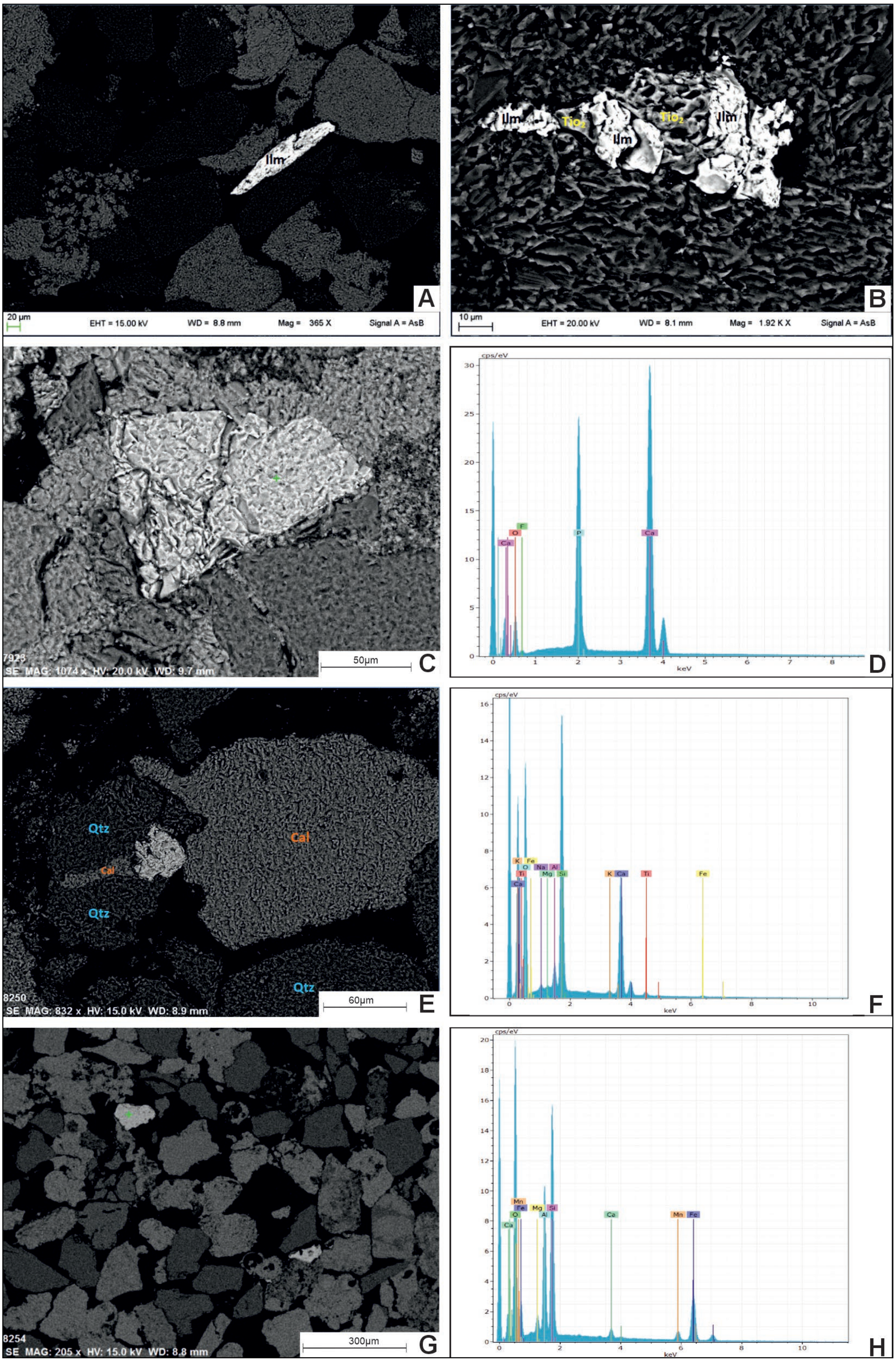

Fig. 13 - Examples of accessory minerals. A) Ilmenite crystal in the form of an elongated lamella (Ilm). Sample MFL5. B) Crystals of ilmenite (Ilm) with titanium oxides (TiO_2) possibly in a lithic fragment. Sample MFL13. C) Fluorapatite crystal and quartz grains embedded in the carbonate cement. Sample MFL12. D) EDS spectrum of a REE free fluorapatite. E) Titanite (bright grain) in a lithic fragment with quartz grains (dark gray, Qtz). Sample MFL5. F) EDS spectrum for titanite. G) Allanite-(Ce) crystal. This epidote group mineral, typical of granites and granitic pegmatites, has been found to contain also significant amounts of Neodymium (Nd), Lanthanum (La), and Thorium (Th), consistently with granitic allanites reported in the literature. Sample MFL1. H) EDS spectrum for allanite-(Ce).

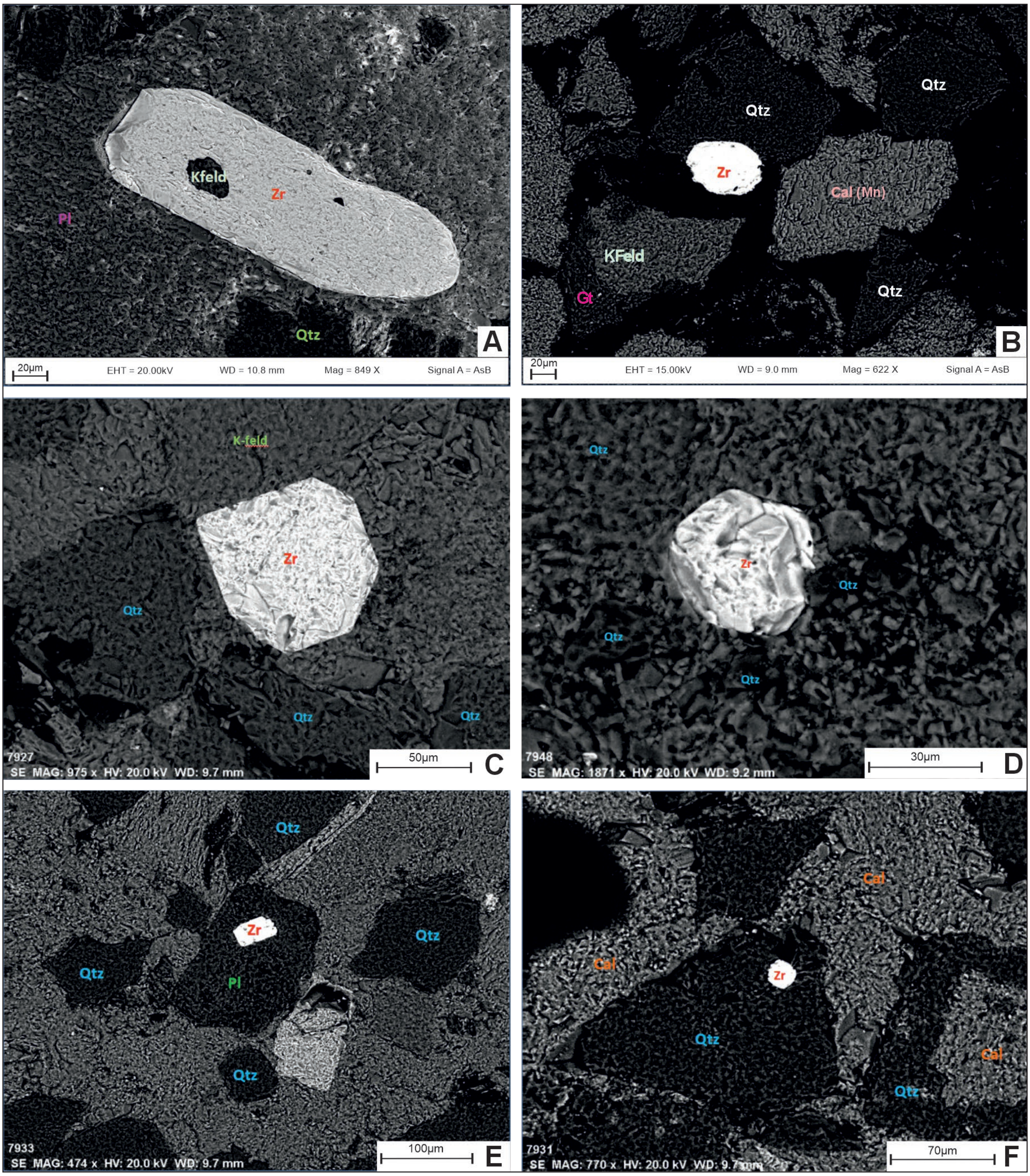

Fig. 14 - Details of zircon crystals from the Spungone Sandstone. Note the different shades of gray which characterized single crystals according to the detected electronic density. A) Euhedral zircon crystal showing a K-feldspar inclusion. Below the zircon it is possible to observe a plagioclase and a quartz crystal on the left side and on the right side, respectively. The size of the zircon is more than 100 µm (scale bar on the left). Sample MFL9. B) Lithic fragment with zircon (Zr) associated with quartz (Qtz). Mn-Calcite (Cal(Mn), quartz grains, and K-feldspar (KFeld) associated with almandine garnet (Gt) are present. Sample MFL5. C) Euhedral zircon grain (bright crystal) embedded in carbonate cement (medium gray) and quartz grains (dark gray). Sample MFL12. D) Zircon crystal (Zr) in the carbonate cement surrounded by quartz grains (Qtz). Sample MFL9. E) Zircon inclusion in a plagioclase (plagioclase composition is $Ab_{79}An_{15}K_{06}$). Sample MFL12. F) Zircon inclusion in a quartz grain (Qtz) embedded in carbonate cement (cal). Sample MFL12.

ent-day Adriatic coastal sediments at water depths ranging from 12 to 17 m (Sabbatini et al. 2016). This organism is capable of chemically selecting minerals, particularly zircon and rutile, through a mecha-

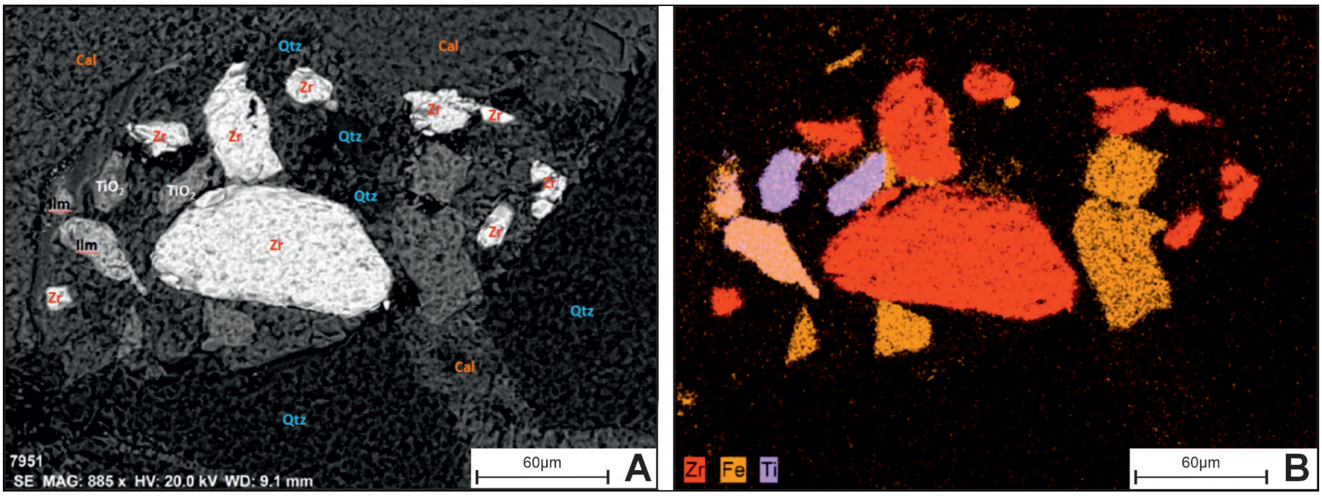

Fig. 15 - A) Unusually high concentration of heavy minerals (zircon, titanium oxides, and ilmenite), contrasting with their extreme rarity in the surrounding sediment, possibly associated with selection and accumulation by representatives of the genus *Psammophaga*, which may preferentially incorporate specific mineral types within the cell. Sample MFL9. B) Elements mapping of the previous image showing the accumulation of zirconia (Zr), iron (Fe) and titanium (Ti).

nism based on electrostatic interactions and is able to retain mineral particles within its cytoplasm.

Discussion

Sequence driving mechanisms

The Pliocene Epoch (5.3-2.6 Ma) represents a critical interval in Earth's history, marked by a major climatic transition from relatively warm conditions to the significantly cooler climates that characterized the Pleistocene (e.g., Miller et al. 2020). This phase of environmental instability coincided with important biotic turnovers, including several molluscan extinction events in the Mediterranean basin (Monegatti & Raffi 2001; Mondanaro et al. 2024). The Zanclean Stage (5.3-3.6 Ma) is generally considered to have been characterized by a globally warm climate (e.g., Passchier et al. 2025). Within this interval, the so-called Pliocene Climatic Optimum (4.4-4.0 Ma) likely represented the warmest phase of the epoch, with global mean temperatures approximately 4 °C higher than present-day values (e.g., Fedorov et al. 2013; Jiménez-Moreno et al. 2019). Despite its climatic significance, this interval has received considerably less attention than the Mid-Piacenzian Warm Period (~3.3-2.9 Ma). During the Zanclean, the Mediterranean region experienced persistently warm sea-surface conditions, with alkenone-derived temperature reconstructions indicating mean values of about 26-26.4 °C (Athanasiou et al. 2017; Beltran et al. 2021). These generally stable warm conditions were intermittently disrupted by short-lived cooling episodes reflecting significant climatic variability during the Early Pliocene (Kontakiotis et al. 2026 and references therein). Although the warm Pliocene interval is generally considered a period of relatively low ice volume, global sea level still fluctuated in response to orbital forcing (e.g., Raymo et al. 2018; Halberstadt et al. 2024). These variations produced short-duration, low-amplitude eustatic oscillations, likely linked to periodic retreat and expansion of the West Antarctic ice sheet (e.g., Gohl et al. 2021), and resulted in repeated inundation and then exposure of marine shelves worldwide. Earlier studies based on geological records from close to the Antarctic coast (e.g., Naish et al. 2009) suggest that Pliocene sea-level variability was predominantly paced by obliquity (~41 kyr). In contrast, more recent high-resolution analyses of far-field, shallow-marine cyclic sedimentary successions from the Whanganui Basin, New Zealand, indicate a more complex pattern, with precession-driven (~20 kyr) oscillations prior to ~3.0 Ma, followed by a transition to obliquity-dominated cyclicity from that time onwards (Grant et al. 2018).

The unconformity-bounded clastic wedges that form the Spungone Sandstone clearly record high-frequency, low-amplitude relative sea-level changes, reflecting a persistent forcing mechanism and suggesting that the same driving factor remained active and consistent throughout the entire period of deposition. The lack of adequate age control prevents a clear discrimination among the roles played by tectonics, eustasy, and sediment supply in shaping its stratigraphic record. However, the distinctive stratigraphic architectural style of these sequences closely resembles that described for high-frequency sequences formed under icehouse conditions characterized by repeated glacio-eustatic sea-level oscillations, such as during the Early Permian (Fielding et al. 2006), the Miocene (Kidwell 1997; Cantalamessa et al. 2007), and the Plio-Pleistocene (e.g., Ito & Katsura 1992; Kitamura et al. 1994; Saul et al. 1999; Massari et al. 2002; Abbott et al. 2005; Cantalamessa et al. 2005; Di Celma et al. 2002, 2005; Naish et al. 2005; Benvenuti et al. 2007; Aldinucci et al. 2019; Dominici et al. 2020; Milaneschi et al. 2026). Accordingly, orbitally driven glacio-eustasy is regarded as the principal mechanism controlling the highly regular cyclicity observed in the studied succession.

During the Pliocene, the overall configuration of the Periadriatic Basin was broadly similar to that of the present day, consisting of a semi-enclosed basin characterized by relatively low wave energy compared to open-marine settings and a generally shallow fair-weather wave base (typically ~10-15 m water depth), although intense storm events could induce seabed reworking down to approximately 20-30 m water depth (Trincardi et al. 1994). Quantifying ancient eustatic changes involves important caveats and assumptions, and estimating the associated relative sea-level rise and fall is challenging. Nevertheless, the abrupt shallowing recorded across wave-ravinement surfaces separating the lower from the middle shoreface facies associations is estimated to have been at least 15 m. This value is consistent with multi-meter-scale estimates of Pliocene glacial-interglacial sea-level variability, including an average amplitude of 13 ± 5 m during the mid-Piacenzian Warm Period (3.3-3.0 Ma; Grant et al. 2019) and of 5-20 m, occasionally peaking at up to 25 m, during the warmer Pliocene Climatic Optimum (4.5-3.0 Ma; Dumitru et al. 2019; Clark et al. 2024). As such, these thin, asymmetric, top-truncated sequences are interpreted as recording eustatic high-frequency, low-amplitude sea-level changes associated with contemporaneous glacial expansion and retreats, whereas accommodation space for their preservation and protection from subsequent erosion, was provided by moderate rates of tectonic subsidence (Kidwell et al. 1997; Fielding et al. 2006). The development of thick, upward-deepening successions of shoreface deposits suggests that sedimentation rates were sufficient to almost keep pace with, but not exceed, the development of accommodation space during long-term base-level rise (Bourgeois 1980; Edwards et al. 2005; Di Celma & Cantalamessa 2007; Jones et al. 2018; Zecchin et al. 2024). The rapid deepening to bathyal depths documented at the upward transition of the Spungone Sandstone into the mud-prone Argille Azzurre Formation sensu stricto reflects a pronounced increase in the accommodation to supply ratio, possibly governed by a significant increase of subsidence rates.

Zecchin et al. (2024) documented a highly cyclothemic, mixed siliciclastic-carbonate shallow-marine succession within the upper Zanclean Belvedere Formation of the Crotone Basin (southern Italy). The succession, deposited in half-graben sub-basins characterized by relatively rapid subsidence, is characterized by meter- to decameter-scale, high-frequency depositional sequences broadly coeval with those recognized in the Spungone Sandstone (Zecchin & Caffau 2012). In that case, each sequence is bounded by ravinement surfaces and displays an internal symmetric architecture comprising a transgressive systems tract overlain by a sediment-driven highstand systems tract of similar thickness. Based on the internal architecture of these high-frequency sequences, marked by the regular alternation of transgressive and highstand systems tracts and by the lack of falling-stage and lowstand deposits, Zecchin et al. (2024) interpreted the cyclicity of the Belvedere Formation as the product of precession-driven climatic forcing. According to this interpretation, the high rates of subsidence in the Crotone Basin likely suppressed glacio-eustatic sea-level oscillations, leading to a persistent relative sea-level rise. In this context, climate-controlled changes in the rate of sediment supply, linked to alternating dry and wet phases, represented the main control on the formation of supply-driven depositional sequences (Di Celma & Cantalamessa 2007; Burgess & Prince 2015) and sequence-bounding ravinement surfaces. This mechanism of sequence development has important implications for sediment dispersal to distal deep-marine settings and suggests that, during deposition of the Belvedere Formation, most of the sand was permanently retained within shallow-water half-grabens, which primarily acted as the ultimate sinks for sediment delivered from up-dip areas, while only minor volumes were transferred to deeper offshore environments.

The Spungone Sandstone differs from the Belvedere Formation in that its depositional sequences developed under the control of relative sea-level fluctuations driven by the interplay between low-amplitude, high-rate global eustatic changes and moderate subsidence rates. As a result, its stratigraphic record is fragmentary, with depositional sequences that are incomplete and preserve only a partial record of relative sea-level changes in which only the transgressive tract survives, while sequence boundaries record periods of erosion and sediment bypass toward more distal sectors of the depositional system. In this case, during deposition of the Spungone Sandstone the internal margin of the Periadriatic Basin acted mainly as a transfer zone involving temporary storage for sediment in transit through the sediment dispersal system, delaying and attenuating the movement of sediment from its source to its final deep-marine depositional sink.

Compositional mix deposits

The Spungone Sandstone consists of mixed terrigenous (extrabasinal) and parautochthonous skeletal (intrabasinal) particles of both bioclastic and peloidal origin that were accumulated contemporaneously in time and space (compositional mixing of Chiarella et al. 2017). At this stage, the most plausible source of the lithic and mineral components is the reworking (cannibalisation) of the Messinian turbidite complex of the Laga Formation. In fact, the petrographic composition of the Laga sediments, directly overlain by the Spungone Sandstone and exposed immediately west of the studied outcrop section, indicates a dominant metamorphic provenance linked to the Alpine domain (Stalder et al. 2018). In particular, the lower Messinan turbidite sandstones of the ME supersynthem of the Laga Formation display a dominant quartzofeldspatholithic composition (Stalder et al. 2018) and reflect mainly a recycled orogenic source (Dickinson 1985; Garzanti 2019). The Laga lithic fraction is dominated by metamorphic components, mainly gneiss and schists, with variable amounts of quartz and feldspars, and subordinate sedimentary particles, chiefly extrabasinal carbonates. The largest $^{238}U/^{206}Pb$ age population of detrital zircons in the Laga Formation ranges from 223 to 323 Ma and exhibits a Permian peak at 278 Ma, along with several subordinate peaks spanning the intervals 390-536 Ma, 572-1080 Ma, 1414-1968 Ma, and 2363-2592 Ma (Stalder et al. 2018). The composition of sandstones and zircon U-Pb geochronology indicate a distal, predominantly metamorphic source likely resulting from the shedding of sediments from the Central and Southern Alps (Valloni et al. 2002; Stalder et al. 2018). The heavy mineral suite in the sandstones of the ME supersynthem of the Laga Formation includes garnet, epidote, zoisite, apatite, staurolite, tourmaline, kyanite, blue amphibole, chloritoid, alanite, as well as ultradense minerals, such as rutile, sphene, and zircon.

Although limited in number and not statistically significant, U-Pb geochronological data from the three zircon grains analyzed in the Spungone Sandstone are consistent with the main Permian peak and one of the secondary peaks identified within the Laga succession. Together with the overall petrographic and mineralogical characteristics of the analyzed samples, these data constrain the sedimentary provenance of the Spungone Sandstone, supporting the interpretation that the lower Messinian Laga arenites exposed immediately west of the study area, represent a likely source of its detrital fraction. This interpretation is further reinforced by the occurrence of metamorphic accessory minerals, including rutile, monazite, and xenotime, within the Spungone's heavy mineral suite. The significant proportion of reworked terrigenous material supplied to the Spungone depositional system by the Laga Formation was substantially diluted by lithic detritus derived from the erosional unroofing of the adjacent Apennine orogenic belt. Those sediments were composed primarily of framework grains of carbonate SRFs and chert, and their mixing with material derived from erosion of the Laga Formation produced the grain populations observed in the Spungone Sandstone (Fig. 12). Collectively, the appreciable reduction of feldspars, some reduction of MRFs, an uptick in SRFs, and a complete lack of VRFs, resulted in a shift of detrital modes within the recycled orogen field toward the lithic (L) endmember on the QtFL plot, and away from arc and continental fields on that and the other ternary plots, since there was little or no input of sediments derived from basement uplift or from magmatic arc sources.

Conclusions

Detailed examination of vertical cliffs in the surroundings of the Montefalcone Appennino village provides stratigraphic and sedimentologic insights into the depositional conditions under which upper Zanclean strata of the Spungone Sandstone were deposited. The studied succession was thoroughly described from a sedimentological perspective and subsequently interpreted within a high-resolution sequence stratigraphic framework to identify the depositional environments in relation to relative sea-level changes. Although the 130 m-thick stratigraphic succession appears initially to be relatively monotonous, with little obvious vertical cyclicity evident from grain-size variations, its internal architecture exhibits a composite organization, characterized by a regular vertical repetition of facies associations and low-angle stratigraphic discontinuities that partition the Spungone Sandstone into a series of unconformity-bounded stratal units. Based on systematic changes in sedimentary facies, eight meter- to decameter-scale high-frequency sequences have been identified. They are incomplete in terms of systems tracts and are top-truncated, with a fundamental sedimentary organization characterized by an upward-deepening, transgressive facies succession. Sequences were deposited in shoreface settings as the shoreline migrated repeatedly back and forth across the basin margin in response to high-frequency, low-amplitude sea-level changes, and are separated by transgressively modified sequence boundaries that record only minor facies-tract dislocations.

Two variants of sequence architecture (motif) can be identified, reflecting differences in the dominant processes operating within the lower shoreface and expressed in two end-member facies successions, namely weakly storm-influenced and strongly storm-dominated shoreface sequences. The ultimate cause of this shift in depositional regime is not currently fully constrained and remains unclear. However, it may be plausibly related to variations in climatic forcing, influencing storm frequency and intensity, as well as changes in coastal morphology, which would affect wave energy dissipation and sediment accommodation patterns along the shoreline.

The broad-scale architecture of the Spungone Sandstone is aggradational and records a phase of overall long-term relative sea-level rise, intermittently punctuated by higher-frequency, low-amplitude glacio-eustatic fluctuations that provided a mechanism for generating repetition of stratigraphic patterns. The asymmetrical, top-truncated architecture of component sequences, expressed by retrogradational sediment wedges, is consistent with deposition in a low-accommodation nearshore setting that prevented the preservation of complete stratal units in the stratigraphic record and produced a thick, cyclical stack of shoreface sandstones. Such a thick succession of aggraded shorefaces supports the interpretation that the Spungone Sandstone represents a time of balance between sediment supply and subsidence-induced accommodation space that precedes pronounced retrogradation associated with increasing rates of basin subsidence.

Mineralogical and modal composition data obtained from sandstone samples indicate that sediments of the Spungone Sandstone were derived from two different main sources. The relative proximity of the Messinian Laga Formation to the study area, coupled with interpretations of eastward directed sediment transport in the area during the Pliocene, suggests that this unit is a likely source for the abundant monocrystalline quartz and for the MRFs in the Spungone samples. The carbonate SRFs are extrabasinal and were sourced from the Apennine orogen, as were many of the chert framework grains, with both coming from uplift and erosion of the Mesozoic-Cenozoic cherty carbonates that are the predominant lithologies in the Umbria-Marche succession, which is exposed in the Sibillini region of the Apennines to the west of the Montefalcone Appennino area. The angular to subangular texture of most quartz grains indicates that transport distances, either linear (e.g. the syn-orogenic sediment routing fluvial systems) or oscillatory (beach and nearshore marine systems), were inadequate to produce appreciable rounding of the quartz. Common intrabasinal bioclastic and peloidal sediment, along with sparse glauconite, which is present both as framework grains and rare pore-reducing cement in some bioclasts, attest to the final depositional environment being in a shallow-marine setting.

Acknowledgments: We would like to express our gratitude to the Museo Comunale dei Fossili e dei Minerali - Museo dell'Alamanno of Montefalcone Appennino and the Museo dei Fossili e dei Minerali of Smerillo for generously providing access to their fossil mollusk collections and for their valuable assistance throughout this study.

We are also grateful to Prof. Coccioni for his invaluable contribution in classifying the fossil mollusks housed in the Museo dell'Alamanno of Montefalcone Appennino. We thank two anonymous reviewers and the Editor Luca Martire for helpful and constructive comments during the review process. This research has been supported by the funds of CARG Project - Geological Map of Italy 1:50,000 (Sheet 326 - Ascoli Piceno) and of James Madison University's College of Science & Mathematics Research Stimulus Program, and University Programs Faculty Council.

Data Availability Statement. The data supporting the results of this research are available upon request. Interested researchers may contact the corresponding author to obtain access.

References

Abbott S.T. (1998) - Transgressive systems tract and onlap shellbeds from Mid-Pleistocene sequences, Wanganui Basin, New Zealand. *Journal of Sedimentary Research*, 68: 253-268. https://doi.org/10.2110/jsr.68.253.

Abbott S.T., Naish T.R., Carter R.M. & Pillans B.J. (2005) - Sequence stratigraphy of the Nukumaruan Stratotype (Pliocene-Pleistocene, c. 2.08-1.63 Ma), Wanganui Basin, New Zealand. *Journal of the Royal Society of New Zealand*, 35: 123-150. https://doi.org/10.1080/03014223.2005.9517779.

Alagna K.E., Petrelli M., Perugini D. & Poli G. (2008) - Micro-analytical zircon and monazite U-Pb isotope dating by Laser Ablation-Inductively Coupled Plasma-Quadrupole Mass Spectrometry. *Geostandards and Geoanalytical Research*, 32: 103-120. https://doi.org/10.1111/j.1751-908X.2008.00866.x.

Aldinucci M., Benvenuti M., Andreetta A., Dominici S., Foresi L.M., Carnicelli S. & Martini I. (2019) - Composite sequence stratigraphic patterns in alluvial to shallow-marine successions: Examples from the Piacenzian of the Valdelsa Basin (Central Italy). *Sedimentary Geology*, 388: 99-113. https://doi.org/10.1016/j.sedgeo.2019.05.005.

Allen P.A., Michael N.A., D'Arcy M., Roda-Boluda D.C., Whittaker A.C., Duller R.A. & Armitage J.J. (2017) - Fractionation of grain size in terrestrial sediment routing systems. *Basin Research*, 29: 129-248. https://doi.org/10.1111/bre.12172.

Anthony E.J. & Aagaard T. (2020) - The lower shoreface: morphodynamics and sediment connectivity with the upper shoreface and beach. *Earth-Science Reviews*, 210: 103334. https://doi.org/10.1016/j.earscirev.2020.103334.

Argnani A. & Ricci Lucchi F. (2001) - Tertiary siliciclastic turbidite systems of the Northern Apennines. In: Vai G.B. & Martini I.P. (Eds) - Anatomy of an Orogen: the Apennines and Adjacent Mediterranean Basins. Springer, Dordrecht, 327-349 pp.. https://doi.org/10.1007/978-94-015-9829-3_19.

Arnott R.W.C. (1993) - Quasi-planar-laminated sandstone beds of the Lower Cretaceous Bootlegger Member, Northcentral Montana: evidence of combined-flow sedimentation. *Journal of Sedimentary Petrology*, 63: 488-494. https://doi.org/10.1306/D4267B31-2B26-11D7-8648000102C1865D.

Artoni A. (2007) - Growth rates and two-mode accretion in the outer orogenic wedge-foreland basin system of Central Apennine (Italy). *Bollettino della Società Geologica Italiana*, 126: 531-556.

Artoni A. (2013) - The Pliocene-Pleistocene stratigraphic and tectonic evolution of the Central sector of the Western Periadriatic Basin of Italy. *Marine and Petroleum Geology*, 42: 82-06. https://doi.org/10.1016/j.marpetgeo.2012.10.005.

Athanasiou M., Bouloubassi I., Gogou A., Klein V., Dimiza D.M., Parinos C., Skampa E. & Triantaphyllou M.V. (2017) - Sea surface temperatures and environmental conditions during the "warm Pliocene" interval (~4.1–3.2 Ma) in the Eastern Mediterranean (Cyprus). *Global and Planetary Change*, 150: 46-57. https://doi.org/10.1016/j.gloplacha.2017.01.008.

Beltran C., Sicre M.A., Ohneiser C. & Sainz M. (2021) - A composite Pliocene record of sea surface temperature in the Central Mediterranean (Capo Rossello composite section-South Sicily). *Sedimentary Geology*, 420: 105921. https://doi.org/10.1016/j.sedgeo.2021.105921.

Benvenuti M., Bertini A., Conti C. & Dominici S. (2007) - Integrated analyses of litho- and biofacies in a Pliocene cyclothemic, alluvial to shallow marine succession (Tuscany, Italy). *Geobios*, 40: 143-158. https://doi.org/10.1016/j.geobios.2006.08.001.

Bigi S., Calamita F., Cello G., Centamore E., Deiana G., Paltrinieri W., Pierantoni P.P. & Ridolfi M. (1999) - Tectonics and sedimentation within a Messinian foredeep in the central Apennines, Italy. *Journal of Petroleum Geology*, 22: 5-18. https://doi.org/10.1111/j.1747-5457.1999.tb00456.x.

Bigi S., Casero P. & Ciotoli G. (2011) - Seismic interpretation of the Laga basin; constraints on the structural setting and kinematics of the Central Apennines. *Journal of the Geological Society, London*, 168: 179-190. https://doi.org/10.1144/0016-76492010-084.

Bigi S., Conti A., Casero P., Ruggiero L., Recanati R. & Lipparini L. (2013) - Geological model of the central Periadriatic basin (Apennines, Italy). *Marine and Petroleum Geology*, 42: 107-121. https://doi.org/10.1016/j.marpetgeo.2012.07.005.

Bizzarri R. (2010) - Early Pleistocene rocky coasts (Orvieto area, Western Umbria, Central Italy): facies analysis and sedimentation models. *Italian Journal of Geosciences (Bollettino della Società Geologica Italiana)* 129: 251-268. https://doi.org/10.3301/IJG.2010.02.

Boccaletti M., Ciaranfi N., Cosentino D., Deiana G., Gelati R., Lentini F., Massari F., Moratti G., Pescatore T., Ricci Lucchi F. & Tortorici L. (1990) - Palinspastic restoration and paleogeographic reconstruction of the peri-Tyrrhenian area during the Neogene. *Palaeogeography, Palaeoclimatology, Palaeoecology*, 77: 41-50. https://doi.org/10.1016/0031-0182(90)90097-Q.

Bouma A.H & Scott E.D. (2003) - Source-to-sink: the importance of the updip coastal area in defining deep-water sand characteristics. In: Roberts H.H., Rosen N.C., Fillon R.H. & Anderson J.B. (Eds) - Shelf Margin Deltas and Linked Down Slope Petroleum Systems-Global Significance and Future Exploration Potential. 23rd Annual GCSSEPM Foundation Bob F. Perkins Research Conference, 96-116. https://doi.org/10.5724/gcs.03.23.

Bourgeois J. (1980) - A transgressive shelf sequence exhibiting hummocky stratification: the Cape Sebastian Sandstone (Upper Cretaceous), southwestern Oregon. *Journal of Sedimentary Research*, 50: 681-702. https://doi.org/10.1306/212F7AC2-2B24-11D7-8648000102C1865D.

Bourgeois J. & Leithold E. (1984) - Wave-worked conglomerates: depositional processes and criteria for recognition. In: Koster E.H. & Steel R.J. (Eds) - Sedimentology of Gravels and Conglomerates. Memories of the Canadian Society Petroleum Geologists 10: 331-343.

Burgess P.M. & Prince G.D. (2015) - Non-unique stratal geometries: implications for sequence stratigraphic interpretations. *Basin Research*, 27: 247-365. https://doi.org/10.1111/bre.12082.

Cantalamessa G., Centamore E., Colalongo M.L., Micarelli A., Nanni T., Pasini G., Potetti M. & Ricci Lucchi F. (1986) - Il Plio-Pleistocene delle Marche. In: Centamore E. & Deiana G. (Eds) - La Geologia delle Marche. *Studi Geologici Camerti*, Special Volume, 61-81.

Cantalamessa G., Centamore E., Didaskalou P., Micarelli A., Napoleone G. & Potetti M. (2002) - Elementi di correlazione nella successione marina plio-pleistocenica del bacino Periadriatico marchigiano. *Studi Geologici Camerti*, Nuova Serie 1/2000: 33-49.

Cantalamessa G. & Di Celma C. (2004) - Sequence response to syndepositional regional uplift: insights from high-resolution sequence stratigraphy of late Early Pleistocene strata, Periadriatic Basin, central Italy. *Sedimentary Geology*, 164: 283-309. https://doi.org/10.1016/j.sedgeo.2003.11.003.

Cantalamessa G., Di Celma C. & Ragaini, L. (2005) - Sequence stratigraphy of the Punta Ballena Member of the Jama Formation (Early Pleistocene, Ecuador): insights from integrated sedimentologic, taphonomic and paleoecologic analysis of molluscan shell concentrations. *Palaeogeography, Palaeoclimatology, Palaeoecology*, 216: 1-25. https://doi.org/10.1016/j.palaeo.2004.09.012.

Cantalamessa G., Di Celma C., Ragaini L., Valleri G. & Landini W. (2007) - Sedimentology and high-resolution sequence stratigraphy of the late Middle to Late Miocene Angostura Formation (western Borbón Basin, north-western Ecuador). *Journal of the Geological Society, London*, 164: 653-665. https://doi.org/10.1144/0016-76492006-001.

Carruba S., Casnedi R., Perotti C.R., Tornaghi M. & Bolis G. (2006) - Tectonic and sedimentary evolution of the Lower Pliocene Periadriatic foredeep in Central Italy. *International Journal of Earth Sciences (Geol Rundsch)*, 95: 665-683. https://doi.org/10.1007/s00531-005-0056-4.

Casnedi R. (1983). Hydrocarbon-bearing submarine fan system of Cellino Formation, Central Italy. *AAPG Bulletin*, 3: 359-370. https://doi.org/10.1306/03B5AD18-16D1-11D7-8645000102C1865D.

Casnedi R., Milia M.L. & Rusciadelli G. (2004). Stratigraphic and tectonic evolution of the Pliocene Abruzzi Basin (Central Apennines, Italy). *Italian Journal of Geosciences*, 123: 163-173.

Castelltort S., Fillon C., Lasseur E., Ortiz A., Robin C, Guillocheau F., Tremblin M., Bessin P., Guerit L., Dekoninck A., Allanic C., Gautheron C., Barbarand J., Loget N., Uzel J., Yans J., Briais J., Al-Reda M., Baby G., François T., Roig J.-Y. & Calassou S. (2023) - The Source-to-Sink Vade-mecum: History, Concepts and Tools. SEPM Concepts in Sedimentology and Paleontology, 16: 71 pp. https://doi.org/10.2110/sepmcsp.16.

Cattaneo A. & Steel R.J. (2003) - Transgressive deposits: a review of their variability. *Earth-Science Reviews*, 62: 187-228. https://doi.org/10.1016/S0012-8252(02)00134-4.

Catuneanu O. & Zecchin M. (2013) - High-resolution sequence stratigraphy of clastic shelves II: controls on sequence development. *Marine and Petroleum Geology*, 39: 26-38. http://dx.doi.org/10.1016/j.marpetgeo.2012.08.010.

Cau S., Laini A., Monegatti P., Roveri M., Scarponi D. & Taviani M. (2019) - Palaeoecological anatomy of shallow-water Plio-Pleistocene biocalcarenites (Northern Apennines, Italy). *Palaeogeography, Palaeoclimatology, Palaeoecology*, 514: 838-851. https://doi.org/10.1016/j.palaeo.2018.08.011

Centamore E., Coltorti M., Dramis F., Cantalamessa G., D'Angelo S., Di Lorito L., Sacchi L. & Sposato A. (1982) - Aspetti neotettonici e geomorfologici del foglio 133 - 134, Ascoli Piceno - Giulianova. Contributi conclusivi per la realizzazione della Carta Neotettonica d'Italia, Pubbl. n. 513 del Progetto Finalizzato Geodinamica, sottoprogetto Neotettonica, 371-386.

Centamore E. & Nisio S. (2003) - Significative events in the Periadriatic foredeeps evolution (Abruzzo-Italy). *Studi Geologici Camerti*, 39-48.

Chiarella D., Longhitano S.G. & Tropeano M. (2017) - Types of mixing and heterogeneities in siliciclastic-carbonate sediments. *Marine and Petroleum Geology*, 88: 617-627. http://dx.doi.org/10.1016/j.marpetgeo.2017.09.010.

Clark P.U., Shakun J.D., Rosenthal Y., Pollard D., Hostetler S.W., Köhler P., Bartlein P.J., Gregory J.M., Zhu C., Schrag D.P., Liu Z. & Pisias N.G. (2024) - Global mean sea level over the past 4.5 million years. *Science*, 390: 884-890. https://doi.org/10.1126/science.adv8389.

Clifton H.E. (2003) - Supply, segregation, succession, and significance of shallow marine conglomeratic deposits. *Bulletin of Canadian Petroleum Geology*, 51: 370-388. https://doi.org/10.2113/51.4.370.

Clifton H.E., Hunter R.E. & Gardner J.V. (1988) - Analysis of eustatic, tectonic and sedimentologic influences on transgressive and regressive cycles in the Upper Cenozoic Merced Formation, San Francisco, California. In: Kleinspehn K.L. & Paola C. (Eds) - New Perspectives in Basin Analysis. New York, Springer-Verlag, 109-128.

Coletti G., Borromeo L., Fallati L., Luppichini M., Meroni A., Maspero F., Malinverno E., Bini M., Palli J., Basso D., Vezzoli G., Garzanti E., Bracchi V.A., Savini A., Desbiolles F., Pasquero C., Correggiari A., Cornacchia I., Boschi C., Baneschi I., Cavallo A., Masotta M., Bosio G., Gallerani A., Fusi N., Mariani L., Galli A., Andò S., Bazzicalupo P., Consani S., Lazzarotti M. & Taccola, G. (2025) - Combining instrumental, historical, and coastal marine sedimentary archives to analyse flood variability in northwestern Italy during the last thousand years. *Quaternary Science Advances*, 100289. https://doi.org/10.1016/j.qsa.2025.100289.

Coletti G., Bosio G. & Collareta A. (2021) - Lower Pliocene barnacle facies of western Liguria (NW Italy): A peek into a warm past and a glimpse of our incoming future. *Rivista Italiana di Paleontologia e Stratigrafia*, 127: 103-131. https://dx.doi.org/10.13130/2039-4942/15202.

Coletti G., Bosio G., Collareta A., Bialik O.M., Regattieri E., Cornacchia I., Insacco G. & Buckeridge J. (2024) - Barnacle-rich facies as a tool for palaeoenvironmental reconstructions. *Palaeogeography, Palaeoclimatology, Palaeoecology*, 634: 111914. https://doi.org/10.1016/j.palaeo.2023.111914

Collier R.E.L. (1990). Eustatic and tectonic controls upon Quaternary coastal sedimentation in the Corinth Basin, Greece. *Journal of the Geological Society, London*, 147: 301-314. https://doi.org/10.1144/gsjgs.147.2.0301.

Crescenti U., D'Amato C., Balduzzi A. & Tonna M. (1980) - Il Plio-Pleistocene del sottosuolo abruzzese-marchigiano tra Ascoli Piceno e Pescara. *Geologica Romana*, 19: 63-84.

Crescenti U., Milia M.L. & Rusciadelli G. (2004) - Stratigraphic and tectonic evolution of the Pliocene Abruzzi Basin (Central Apennines, Italy). *Italian Journal of Geosciences*, 123: 163-173.

Dattilo P., Pasi R. & Bertozzi G. (1999) - Depositional and structural dynamics of the Pliocene Peri-Adriatic Foredeep, NE Italy. *Journal of Petroleum Geology*, 22: 19-36. https://doi.org/10.1111/j.1747-5457.1999.tb00457.x

De Celles P.G. (2012) - Foreland basin systems revisited: variations in response to tectonic settings. In: Busby C.J. & Azor A. (Eds) - Tectonics of Sedimentary Basins: Recent Advances. New York, John Wiley & Sons, 405-426. https://doi.org/10.1002/9781444347166.ch20.

Dewey J.F., Helman M.L., Knott S.D., Turco E. & Hutton D.H. (1989) - Kinematics of the western Mediterranean. Geological Society, London, Spec. Publ. 45, 256-283. https://doi.org/10.1144/GSL.SP.1989.045.01.15

Demarest J.M. II & Kraft, J.C. (1987) - Stratigraphic record of Quaternary sea levels: Implications for more ancient strata. In: Nummedal D., Piikey O.H. & Howard J.D. (Eds) - Sea-level Fluctuations and Coastal Evolution. SEPM Spec. Publ. 41, 223-239. https://doi.org/10.2110/pec.87.41.0223.

Di Celma C. (2011) - Sedimentology, architecture, and depositional evolution of a coarse-grained submarine canyon fill from the Gelasian (early Pleistocene) of the Peri-Adriatic basin, Offida, central Italy. *Sedimentary Geology*, 238: 233-253. https://doi.org/10.1016/j.sedgeo.2011.05.003.

Di Celma C. (2025) - Note Illustrative della Carta Geologica d'Italia alla scala 1:50.000, F. 326 Ascoli Piceno. Servizio Geologico d'Italia – ISPRA, 204 pp. https://doi.org/10.15161/oar.it/f2mge-2gp27.

Di Celma C., Artoni A., Jablonska D., Mammoliti E., Malavolta M., Principi M., Caffau M., Didaskalou, P. & Cantalamessa G. (2023) - Pleistocene slope, shallow-marine and continental deposits of eastern central Italy wedgetop basin: a record of sea-level changes and mountain building. *Geological Field Trips and Maps*, 15: 207 pp. https://doi. org/10.3301/GFT.2023.03.

Di Celma C. & Cantalamessa G. (2007) - Sedimentology and high-frequency sequence stratigraphy of a forearc extensional basin: The Miocene Caleta Herradura Formation, Mejillones Peninsula, northern Chile. *Sedimentary Geology*, 198: 29-52. https://doi.org/10.1016/j.sedgeo.2006.11.003.

Di Celma C., Cantalamessa G. & Didaskalou P. (2013) - Stratigraphic organization and predictability of mixed coarse-grained and fine-grained successions in an upper slope Pleistocene turbidite system of the Peri-Adriatic basin. *Sedimentology*, 60: 763-799. https://doi.org/10.1111/j.1365-3091.2012.01359.x.

Di Celma C., Cantalamessa G., Didaskalou P. & Lori P. (2010) - Sedimentology, architecture, and sequence stratigraphy of coarse-grained, submarine canyon fills from the Pleistocene (Gelasian-Calabrian) of the Peri-Adriatic basin, central Italy. *Marine and Petroleum Geology*, 27: 1340-1365. https://doi.org/10.1016/j.marpetgeo.2010.05.011.

Di Celma C., Pieruccini P. & Farabollini, P. (2015) - Major controls on architecture, sequence stratigraphy and paleosols of middle Pleistocene continental sediments ("Qc Unit"), eastern central Italy. *Quaternary Research*, 83: 565-581. https://doi.org/10.1016/j.yqres.2015.01.006.

Di Celma C., Ragaini L., Cantalamessa G. & Curzio, P. (2002) - Shell concentrations as tools in characterizing sedimentary dynamics at sequence-bounding unconformities: examples from the lower unit of the Canoa Formation (Late Pliocene, Ecuador). *Geobios*, 35: 72-85. https://doi.org/10.1016/S0016-6995(02)00049-9.

Di Celma C., Ragaini L., Cantalamessa G. & Landini W. (2005) - Basin physiography and tectonic influence on sequence architecture and stacking pattern: Pleistocene succession of the Canoa Basin (central Ecuador). *Geological Society of America Bulletin*, 117: 1226-1241. https://doi.org/10.1130/B25684.1.

Di Celma C., Teloni R. & Rustichelli A. (2014) - Large-scale stratigraphic architecture and sequence analysis of an early Pleistocene submarine canyon fill, Monte Ascensione succession (Peri-Adriatic central Italy). *International Journal of Earth Sciences*, 103: 843-875. https://doi.org/10.1007/s00531-013-0984-3.

Dickinson W.R. & Suczek C.A. (1979) - Plate tectonics and sandstone compositions. *AAPG Bulletin*, 63: 2164-2182. https://doi.org/10.1306/2F9188FB-16CE-11D7-8645000102C1865D.

Dickinson W.R. (1985) - Interpreting provenance relations from detrital modes of sandstones. In: Zuffa G.G. & Reidel D. (Eds) - Provenance of Arenites. Springer, Dordrecht, 333-361. https://doi.org/10.1007/978-94-017-2809-6_15.

Dickinson W.R. (1988) - Provenance and sediment dispersal in relation to paleotectonics and paleogeography of sedimentary basins. In: Kleinspehn K.L. & Paola C. (Eds) - New Perspectives in Basin Analysis Frontiers in Sedimentary Geology. Springer-Verlag, New York, 3-25. https://doi.org/10.1007/978-1-4612-3788-4_1.

Dickinson W.R., Beard L.S., Brakenridge G.R., Erjavec J.L., Ferguson R.C., Inman K.F., Knepp R.A., Lindberg F.A. & Ryberg P.T. (1983) - Provenance of North American Phanerozoic sandstones in relation to tectonic setting. *Geological Society of America Bulletin*, 94: 222-235. https://doi.org/10.1130/0016-7606(1983)94<222:PON-APS>2.0.CO;2.

Dickson J.A.D. (1965) - A modified staining technique for carbonates in thin section. *Nature*, 205: 587. https://doi.org/10.1038/205587a0.

Di Stefano A., Baldassini N., Raffi I., Fornaciari E., Incarbona A., Negri A., Bonomo S., Villa G., Di Stefano E. & Rio D. (2023) - Neogene-Quaternary Mediterranean calcareous nannofossil biozonation and biochronology: A review. *Stratigraphy*, 20: 259-302. https://dx.doi.org/10.29041/strat.20.4.02.

Doglioni C. (1991) - A proposal for the kinematic modelling of W-dipping subductions - possible applications to the Tyrrhenian-Apennines system. *Terra Nova*, 3: 423-434. https://doi.org/10.1111/j.1365-3121.1991.tb00172.x.

Dominici S., Benvenuti M., Garilli V., Uchman A., Pollina F. & David A. (2020) - Pliocene-Pleistocene stratigraphic paleobiology at Altavilla Milicia (Palermo, Sicily): tectonic, climatic and eustatic forcing. *Bollettino della Società Paleontologica Italiana*, 59: 57-83. https://doi.org/10.4435/BSPI.2020.06.

Dominici S. & Forli M. (2021) - Lower Pliocene molluscs from southern Tuscany (Italy). *Bollettino della Società Paleontologica Italiana*, 60: 69-98. https://doi.org/10.4435/

BSPI.2021.04.

Dott R.H. & Bourgeois J. (1982) - Hummocky stratification: Significance of its variable bedding sequences. *Geological Society of America Bulletin*, 93: 663-680. https://doi.org/10.1130/0016-7606(1982)93<663:HSSOIV>2.0.CO;2.

Dumitru O.A., Austermann J., Polyak V.J., Fornós J.F., Asmerom, Y., Ginés J., Ginés A. & Onac B.P. (2019) - Constraints on global mean sea level during Pliocene warmth. *Nature*, 574: 233-236. https://doi.org/10.1038/s41586-019-1543-2.

Edwards C.M., Howell J.A. & Flint S.S. (2005) - Depositional and stratigraphic architecture of the Santonian Emery Sandstone of the Mancos Shale: Implications for Late Cretaceous evolution of the Western Interior foreland basin of central Utah, U.S.A. *Journal of Sedimentary Research*, 75: 280-299. https://doi.org/10.2110/jsr.2005.021.

Fedorov A.V., Brierley C.M., Lawrence K.T., Liu Z., Dekens P.S. & Ravelo A.C. (2013) -

Patterns and mechanisms of early Pliocene warmth. *Nature*, 496: 43-49. https://doi.org/10.1038/nature12003.

Fielding C.R., Bann K.L., MacEachern J.A., Tye S.C. & Jones B.G. (2006) - Cyclicity in the nearshore marine to coastal, Lower Permian, Pebbley Beach Formation, southern Sydney Basin, Australia: a record of relative sea-level fluctuations at the close of the Late Palaeozoic Gondwanan ice age. *Sedimentology*, 53: 435-463. https://dx.doi.org/10.1111/j.1365-3091.2006.00770.x.

Folk R.L. (1980) - Petrology of sedimentary rocks. Austin, Texas, Hemphill Publishing Co., 182 p.

Folk R.L., Andrews P.B. & Lewis D.W. (1970) - Detrital sedimentary rock classification and nomenclature for use in New Zealand. *New Zealand Journal of Geology and Geophysics*, 13: 937-968. https://doi.org/10.1080/00288306.1970.10418211.

Galloway W.E. & Hobday D.K. (1996) - Terrigenous Shelf Systems. In: Terrigenous Clastic Depositional Systems. Springer, Berlin, Heidelberg, 159-185. https://doi.org/10.1007/978-3-642-61018-9_7.

Garzanti E. (2019) - Petrographic classification of sand and sandstone. *Earth-Science Reviews*, 192: 545-563. https://doi.org/10.1016/j.earscirev.2018.12.014.

Ghibaudo G., Grandesso P., Massari F. & Uchman A. (1996) - Use of trace fossils in delineating sequence stratigraphic surfaces (Tertiary Venetian Basin, northeastern Italy). *Palaeogeography, Palaeoclimatology, Palaeoecology*, 120: 261-279. https://doi.org/10.1016/0031-0182(95)00048-8.

Ghielmi M., Serafini G., Artoni A., Di Celma C. & Pitts A. (2019) - From Messinian to Pleistocene: tettonic evolution and stratigraphic architecture of the central Adriatic Foredeep (Abruzzo and Marche, Central Italy). International Meeting of Sedimentology. Associazione Italiana di Geologia del Sedimentario-GeoSed, 45 pp.

Ghinassi M. (2007) - The effects of differential subsidence and coastal topography on high-order transgressive-regressive cycles: Pliocene nearshore deposits of the Val d'Orcia Basin, Northern Apennines, Italy. *Sedimentary Geology*, 202: 677-701. https://doi.org/10.1016/j.sedgeo.2007.08.002.

Gohl K., Uenzelmann-Neben G., Gille-Petzoldt J., Hillenbrand C.-D., Klages J. P., Bohaty S.M., Passchier S., Frederichs T., Wellner J.S., Lamb R., Leitchenkov G. & IODP Expedition 379 Scientists (2021) - Evidence for a highly dynamic West Antarctic Ice Sheet during the Pliocene. *Geophysical Research Letters*, 48: e2021GL093103. https://doi.org/10.1029/2021GL093103.

Grant G.R., Sefton J.P., Patterson M.O., Naish T.R. Dunbar, G.B. Hayward B.W., Morgans H.E.G., Alloway B.V., Seward D., Tapia C.A., Prebble J.B., Kamp P.J.J., McKay R., Ohneiser C. & Turner G.M. (2018) - Mid- to late Pliocene (3.3-2.6 Ma) global sea-level fluctuations recorded on a continental shelf transect, Whanganui Basin, New Zealand. *Quaternary Science Reviews*, 201: 241-260. https://doi.org/10.1016/j.quascirev.2018.09.044.

Halberstadt A.R.W., Gasson E., Pollard D., Marschalek J. &, DeConto R.M. (2024) - Geologically constrained 2-million-year-long simulations of Antarctic Ice Sheet retreat and expansion through the Pliocene. *Nature Communications*, 15: 7014. https://doi.org/10.1038/s41467-024-51205-z.

Harms J.C., Southard J.B., Spearing D.R. & Walker R.G. (1975) - Depositional environments as interpreted from primary sedimentary structures and stratification sequences. *SEPM Short Course Notes*, 2: 161 pp. https://doi.org/10.2110/scn.75.02.

Hart B.S. & Plint A.G. (1995) - Gravelly shoreface and beachface deposits. In: Plint, A.G. (Ed), Sedimentary Facies Analysis: A tribute to the Research and Teaching of Harold G. Reading. IAS Spec. Publ., 22, 75-99. https://doi.org/10.1002/9781444304091.ch4.

Helland-Hansen W., Sømme T.O., Martinsen O.J., Lunt I. & Thurmond J. (2016) - Deciphering Earth's natural hourglasses: perspectives on source-to-sink analysis. *Journal of Sedimentary Research*, 86: 1008-1033. https://doi.org/10.2110/jsr.2016.56.

Hill P.R., Meule S. & Longuépée H. (2003) - Combined-flow processes and sedimentary structures on the shoreface of the wave-dominated Grande-riviere-de-la-Baleine delta. *Journal of Sedimentary Research*, 73: 217-226. https://doi.org/10.1306/080802730217.

Hitzman M.W. (1999) - Routine staining of drill core to determine carbonate mineralogy and distinguish carbonate alteration textures. *Mineralium Deposita*, 34: 794-798. https://doi.org/10.1007/s001260050240.

Ingersoll R.V. (1983) - Petrofacies and provenance of late Mesozoic forearc basin, northern and central California. *AAPG bulletin*, 67: 1125-1142. https://doi.org/10.1306/03B5B713-16D1-11D7-8645000102C1865D.

Ingersoll R.V. & Suczek C.A. (1979) - Petrology and provenance of Neogene sand from Nicobar and Bengal fans, DSDP sites 211 and 218. *Journal of Sedimentary Research*, 49: 1217-1228. https://doi.org/10.1306/212F78F1-2B24-11D7-8648000102C1865D.

Ito M. & Katsura Y. (1992) - Inferred glacio-eustatic control for high-frequency depositional sequences of the Plio-Pleistocene Kazusa Group, a forearc basin fill in Boso Peninsula, Japan. *Sedimentary Geology*, 80: 67-75. https://doi.org/10.1016/0037-0738(92)90032-M.

James M.R. & Robson S. (2012) - Straightforward reconstruction of 3D surfaces and topography with a camera: accuracy and geoscience application. *Journal of Geophysical Research: Earth Surface*, 117: F03017. https://doi.org/10.1029/2011JF002289.

Jelby M.E., Grundvåg S.-A., Helland Hansen W., Olaussen S. & Stemmerik L. (2020) - Tempestite facies variability and storm-depositional processes across a wide ramp: Towards a polygenetic model for hummocky cross-stratification. *Sedimentology*, 67: 742-781. https://doi.org/10.1111/sed.12671.

Jiménez-Moreno G., Pérez-Asensio J.N., Larrasoaña J.C., Sierro F.J., Garcia-Castellanos D., Salazar Á., Salvany J.M., Ledesma S., Mata M.P. & Mediavilla C. (2019) - Early Pliocene climatic optimum, cooling and early glaciation deduced by terrestrial and marine environmental changes in SW Spain. *Global and Planetary Change*, 180: 89-99. https://doi.org/10.1016/j.gloplacha.2019.06.002.

Jones M.T., Dashtgard S.E. & MacEachern J.A. (2018) - A conceptual model for the preservation of thick, transgressive shoreline successions: examples from forearc Nanaimo Basin, British Columbia, Canada. *Journal of Sedimentary Research*, 88: 811-826. http://dx.doi.org/10.2110/jsr.2018.40.

Kabekkodu S., Dosen A. & Blanton T. (2024) - PDF-5+: a comprehensive Powder Diffraction File™ for materials characterization. *Powder Diffraction*, 39: 47-59. http://dx.doi.org/10.1017/S0885715624000150.

Kidwell S.M. (1993) - Taphonomic expressions of sedimentary hiatuses: field observations on bioclastic concentrations and sequence anatomy in low, moderate and high subsidence settings. *Geologische Rundschau*, 82: 189-202. https://doi.org/10.1007/BF00191825.

Kidwell S.M. (1997) - Anatomy of extremely thin marine sequences landward of a passive-margin hinge zone: Neogene Calvert Cliffs succession, Maryland, U.S.A. *Journal of Sedimentary Research*, 67: 322-340. https://doi.org/10.1306/D4268563-2B26-11D7-8648000102C1865D

Kidwell S.M. & Holland S.M. (1991) - Field description of coarse bioclastic fabrics. *Palaios*, 6: 426-434. https://doi.org/10.2307/3514967.

Kitamura A., Kondo Y., Sakai H. & Horii M. (1994) - Cyclic changes in lithofacies and molluscan content in the early Pleistocene Omma Formation, Central Japan related to the 41.000-year orbital obliquity. *Palaeogeography, Palaeoclimatology, Palaeoecology*, 112: 345-361. https://doi.org/10.1016/0031-0182(94)90080-9.

Kondo Y., Abbott S.T., Kitamura A., Kamap P.J.J., Naish T.R., Katamataki T. & Saul G.S. (1998) - The relationship between shellbed type and sequence architecture: examples from Japan and New Zealand. *Sedimentary Geology*, 122: 109-127. https://doi.org/10.1016/S0037-0738(98)00101-8.

Kontakiotis G., Quillévéré F., Vasiliev I., Antonarakou A., Triantaphyllou M., Besiou E., Skampa E., Moissette P., Vinçon-Laugier A. & Cornée J.-J. (2026) - Climate-modulated and tectonics-induced controls on the paleoceanographic evolution of the southeastern Mediterranean Sea across the Zanclean-Piacenzian transition. *Global and Planetary Change*, 263: 105531. https://doi.org/10.1016/j.gloplacha.2026.105531.

Kreisa R.D. (1981) - Storm-generated sedimentary structures in subtidal marine facies with examples from the Middle and Upper Ordovician of southwestern Virginia. *Journal of Sedimentary Petrology*, 51: 823–848. https://doi.org/10.1306/212F7DBF-2B24-11D7-8648000102C1865D.

Lirer F., Foresi L.M., Iaccarino S.M., Salvatorini G., Turco E., Cosentino C., Sierro F.J. & Caruso A. (2019) - Mediterranean Neogene planktonic foraminifer biozonation and biochronology. *Earth-Science Reviews*, 196: 102869. https://doi.org/10.1016/j.earscirev.2019.05.013.

MacEachern J.A. & Bann K.L. (2008) - The role of ichnology in refining shallow marine facies models. In: Hampson G.J., Steel R.J., Burgess P.M. & Dalrymple R.W. (Eds) - Recent Advances in Models of Siliciclastic Shallow-Marine Stratigraphy. SEPM Spec. Publ. 90: 73-116. https://doi.org/10.2110/pec.08.90.0073.

MacEachern J.A., Dashtgard S.E., Knaust D., Catuneanu O., Bann K.L. & Pemberton S.G. (2012) & Sequence stratigraphy: Trace fossils as indicators of sedimentary environments. In: Knaust D. & Bromley R.G. (Eds) - Developments in Sedimentology 64: 157-194. Amsterdam, Elsevier. https://doi.org/10.1016/B978-0-444-53813-0.00006-X.

MacEachern J.A. & Pemberton, S.G. (1992) - Ichnological aspects of Cretaceous shoreface successions and shoreface variability in the Western Interior Seaway of North America. In: Pemberton S.G. (Ed) - Applications of Ichnology to Petroleum Exploration: A Core Workshop. SEPM Core Workshop, 17: 57-84. https://doi.org/10.2110/cor.92.01.0057.

Malinverno A. & Ryan W.B.F. (1986) - Extension in the Tyrrhenian Sea and shortening in the Apennines as result of arc migration driven by sinking of the lithosphere. *Tectonics*, 5: 227-245. https://doi.org/10.1029/TC005i002p00227.

Marsaglia K.M., Tentori D., Shorrock A., Franco A., Adedeji A. & Strachan L.J. (2026) - New insights on routing of sand across and along the Hikurangi subduction margin add complexity to the source-to-sink paradigm. *Journal of Sedimentary Research*, 96: 610-633. https://doi.org/10.2110/jsr.2025.097.

Mascarini A. (1880) - Su alcuni fossili terziari di Monte Falcone (nella provincia di Ascoli Piceno): contribuzione alla paleontologia marchigiana. *Bollettino del R. Comitato geologico d'Italia*, 7-8: 357-367.

Massari F. (2021) - Storm signature in the Messinian and Pleistocene record of drift- and swash-aligned Mediterranean gravel beaches. Role of precession-driven intensification of the Mediterranean cyclogenesis. *Journal of Mediterranean Earth Sciences*, 13: 31-76. https://doi.org/10.13133/2280-6148/17480.

Massari F. & D'Alessandro A. (2010) - Icehouse, cool-water carbonate ramps: the case of the Upper Pliocene Capodarso Fm (Sicily): role of trace fossils in the reconstruction of growth stages of prograding wedges. *Facies*, 56: 47-58. https://doi.org/10.1007/s10347-009-0191-7.

Massari F., Rio D., Sgavetti M., Prosser G., D'Alessandro A., Asioli A., Capraro L., Fornaciari E. & Tateo F. (2002) - Interplay between tectonics and glacio-eustasy: Pleistocene succession of the Crotone basin, Calabria (southern Italy). *Geological Society of America Bulletin*, 114: 1183-1209. https://doi.org/10.1130/0016-7606(2002)114<1183:IBTAGE>2.0.CO;2.

Mazumder R. (2017) - Sediment provenance. In: Sediment Provenance: Influences on Compositional Change from Source to Sink. Elsevier, pp. 1-4. https://doi.org/10.1016/B978-0-12-803386-9.00001-0.

Milaneschi L., Cornamusini G., Conti P., Martini I., Maffei J., Cifelli F., Mattei M., Da Prato S., Alçiçek M.C. & Foresi L.M. (2026) - Unveiling "Mid-Pliocene Warm Period" dynamics through multiproxy stratigraphic analysis: The Valdelsa Basin in Northern Apennines – Italy as a key archive. *Palaeogeography, Palaeoclimatology, Palaeoecology*, 694: 113744. https://doi.org/10.1016/j.palaeo.2026.113744.

Miller K.G., Schmelz W.J., Browning J.V., Kopp R.E., Mountain G.S. & Wright J.D. (2020) - Ancient sea level as key to the future. *Oceanography*, 33: 32-41. https://doi.org/10.5670/oceanog.2020.224.

Mondanaro A., Dominici S. & Danise S. (2024) - Response of Mediterranean Sea bivalves to Pliocene-Pleistocene environmental changes. *Palaeontology*, 67: 12696. https://doi.org/10.1111/pala.12696.

Monegatti P. & Raffi S. (2001) - Taxonomic diversity and stratigraphic distribution of Mediterranean Pliocene bivalves. *Palaeogeography, Palaeoclimatology, Palaeoecology*, 165: 171-193. https://doi.org/10.1016/S0031-0182(00)00159-0.

Myrow P.M. & Southard J.B. (1991) - Combined-flow model for vertical stratification sequences in shallow marine storm-deposited beds. *Journal of Sedimentary Research*, 61: 202-210. https://doi.org/10.1306/D42676D1-2B26-11D7-8648000102C1865D.

Naish T., Powell R., Levy R., Wilson G., Scherer R., Talarico F., Krissek L., Niessen F., Pompilio M., Wilson T., Carter L., DeConto R., Huybers P., McKay R., Pollard D., Ross J., Winter D., Barrett P., Browne G., Cody R., Cowan E., Crampton J., Dunbar G., Dunbar N., Florindo F., Gebhardt C., Graham I., Hannah M., Hansaraj D., Harwood D., Helling D., Henrys S., Hinnov L., Kuhn G., Kyle P., Laufer A., Maffioli P., Magens D., Mandernack K., McIntosh W., Millan C., Morin R., Ohneiser C., Paulsen T., Persico D., Raine I., Reed J., Riesselman C., Sagnotti L., Schmitt D., Sjunneskog C., Strong P., Taviani M., Vogel S., Wilch T. & Williams T. (2009) - Obliquity-paced Pliocene West Antarctic ice sheet oscillations. *Nature*, 458: 322-328. https://doi.org/10.1038/nature07867.

Nalin R. & Massari F. (2009) - Facies and stratigraphic anatomy of a temperate carbonate sequence (Capo Colonna terrace, late Pleistocene, southern Italy). *Journal of Sedimentary Research*, 79: 210-225. https://doi.org/0.2110/jsr.2009.027.

Nalin R., Massari F. & Zecchin, M. (2007) - Superimposed cycles of composite marine terraces: the example of Cutro terrace (Calabria, southern Italy). *Journal of Sedimentary Research*, 77: 340–354. https://doi.org/10.2110/jsr.2007.030.

Nayak K., Garzanti E., Lin A. T.S. & Castelltort, S. (2022) - Taiwan river muds from source to sink: Provenance control, inherited weathering, and offshore dispersal pathways. *Sedimentary Geology*, 438, 106199. https://doi.org/10.1016/j.sedgeo.2022.106199.

Neal J.E., Abreu V., Bohacs K.M., Feldman H.R. & Pederson K.H. (2016) - Accommodation succession (δA/δS) sequence stratigraphy: observational method, utility and insights into sequence boundary formation. *Journal of the Geological Society, London*, 173: 803-816. https://doi.org/10.1144/jgs2015-165.

Nemec W. & Steel R.J. (1984) - Alluvial and coastal conglomerates: their significant features and some comments on gravelly mass-flow deposits. In: Koster E.H. & Steel R.J. (Eds) - Sedimentology of Gravels and Conglomerates. Canadian Society of Petroleum Geologists Memoir 10, pp. 1-31.

Nesbit P.R., Durkin P.R., Hugenholtz C.H., Hubbard S.M. & Kucharczyk M. (2018) - 3-D stratigraphic mapping using a digital outcrop model derived from UAV images and structure-from-motion photogrammetry. *Geosphere*, 14: 2469-2486. https://doi.org/10.1130/GES01688.1.

Nummedal D. & Swift D.J.P. (1987) - Transgressive stratigraphy at sequence-bounding unconformities: some principles derived from Holocene and Cretaceous examples. In: Nummedal D., Pilkey O.H. & Howard J.D. (Eds) - Sea-Level Fluctuation and Coastal Evolution. SEPM, Spec. Publ. 41, pp. 241-259. https://doi.org/10.2110/pec.87.41.0241.

Okwara I.C., Hampson G.J., Whittaker A.C. & Roberts G.G. (2025) - Downsystem grain-size trends and mass balance of an ancient wave-influenced sediment routing system: Middle Jurassic Brent Delta, northern North Sea, offshore UK and Norway. *Sedimentologika*, 3: 1-27. https://doi.org/10.57035/journals/sdk.2025.e31.1336

Ori G.G. & Friend P.F. (1984) - Sedimentary basins formed and carried piggyback on active thrust sheets. *Geology*, 12: 475-478. https://doi.org/10.1130/0091-7613(1984)12<475:SBFACP>2.0.CO;2.

Ori G.G., Serafini G., Visentin C., Ricci Lucchi F., Casnedi R. & Calalongo M. (1991) - The Pliocene-Pleistocene Adriatic Foredeep (Marche and Abruzzo, Italy): an integrated approach to surface and subsurface geology. 3rd EAPG Conference, Florence, AGIP-EAPG.

Ori G.G., Serafini G., Visentin C., Ricci Lucchi F., Casnedi R., Colalongo M.L. & Mosna S. (1993) - Depositional history of the Plio-Pleistocene Adriatic foredeep (Central Italy) from surface and subsurface data. In: Spencer, A.M. (Ed) - Generation, Accumulation and Production of Europe's Hydrocarbons III. Special Publication of the European Association of Petroleum Geoscientists, vol. 3, pp. 233-258. Springer, Berlin, Heidelberg. https://doi.org/10.1007/978-3-642-77859-9_19.

Over J.R., Ritchie A.C., Kranenburg C.J., Brown J.A., Buscombe D., Noble T., Sherwood C.R., Warrick J.A. & Wernette P.A. (2021) - Processing coastal imagery with Agisoft Metashape Professional Edition, version 1.6-Structure from motion workflow documentation: U.S. Geological Survey Open-File Report 2021–1039, 46, https://doi.org/10.3133/ofr20211039.

Passchier S., Hillenbrand C.D., Hemming S., Ehrmann W., Frederichs T., Bohaty S.M., Leon R., Libman-Roshal O., Mino-Moreira L., Gohl K. & Wellner J. (2025) - West Antarctic ice retreat and paleoceanography in the Amundsen Sea in the warm early Pliocene. *Nature Communications*, 16: 5609. https://doi.org/10.1038/s41467-025-60772-8.

Patacca E., Sartori R. & Scandone P. (1990) - Tyrrhenian basin and Apenninic arcs: Kinematic relations since Late Tortonian times. *Memorie della Societa Geologica Italiana*, 45: 425-451.

Pavia G., Dulai A., Festa A., Gennari R., Pavia M. & Carnevale G. (2022) - Palaeontology of the Upper Pliocene marine deposits of Rio Vaccaruzza, Villalvernia (Piedmont, NW Italy). Rivista Italiana di Paleontologia e Stratigrafia, 128: 129-210. http://doi.org/10.54103/2039-4942/15178.

Pedini M. (2025) - Modello geologico 3D della Carta Geologica d'Italia alla scala 1:50.000. Foglio 326 "Ascoli Piceno". ISPRA. http://doi.org/10.15161/oar.it/tdq5a-nmx86.

Pedini M., Cella F., Di Celma C., Mazzoli S., Pierantoni P.P. & Zambrano M. (in press) - Detachment- vs. crustal ramp-dominated thrusting in the Umbria-Marche Apennines, Italy. *Geological Society of America Bulletin*,

Pemberton S.G. & MacEachern J.A. (1995) - The sequence stratigraphic significance of trace fossils: examples from the Cretaceous foreland basin of Alberta, Canada. In: Van Wagoner J.C. & Bertram G. (Eds) - Sequence stratigraphy of foreland basin deposits-outcrop and subsurface examples from the Cretaceous of North America. AAPG Memoir, 64: pp. 429-475. https://doi.org/10.1306/M64594C15.

Pemberton S.G., MacEachern J.A. & Frey R.W. (1992) - Trace fossil facies models: environmental and allostratigraphic significance. In: Walker R.G. & James N.P. (Eds) - Facies Models: Response to Sea Level Change. Geological Association of Canada, Toronto, pp. 47-72.

Pemberton S.G., MacEachern J.A., Dashtgard S.E., Bann K.L., Gingras M.K. & Zonneveld J.-P. (2012) - Shorefaces. In: Knaust D. & Bromley R.G. (Eds) - Trace Fossils as Indicators of Sedimentary Environments. Developments in Sedimentology, 64: pp. 563-603. https://doi.org/10.1016/B978-0-444-53813-0.00019-8.

Pitts A., Casciano C.I., Patacci M., Longhitano S.G., Di Celma C. & McCaffrey W.D. (2017) - Integrating traditional field methods with emerging digital techniques for enhanced outcrop analysis of deep water channel-fill deposits. *Marine and Petroleum Geology*, 87: 2-13. https://doi.org/10.1016/j.marpetgeo.2017.05.001.

Plint A.G. (2010) - Wave- and storm-dominated shoreline and shallow-marine systems. In: James N.P. & Dalrymple R.W. (Eds) - Facies Models 4, Geological Association of Canada, Newfoundland, pp. 167-199.

Pomar L. & Tropeano M. (2001) - The Calcarenite di Gravina Formation in Matera (southern Italy): New insights for coarse-grained, large-scale, cross-bedded bodies encased in offshore deposits. *AAPG Bulletin*, 85: 661-689. https://doi.org/10.1306/8626C979-173B-11D7-8645000102C1865D.

Puig López J.P. & Howell J. (2024) - Facies models for rocky shorelines and their application to transgressed basement highs in the North Sea. *Journal of the Geological Society*, *London*, 18: jgs2024-012. https://doi.org/10.1144/jgs2024-012.

Raymo M.E., Kozdon R., Evans D., Lisiecki L. & Ford H.L. (2018) - The accuracy of mid-Pliocene $\delta^{18}O$-based ice volume and sea level reconstructions. Earth-Science Reviews, 177: 291-302. https://doi.org/10.1016/j.earscirev.2017.11.022.

Reading H.G. & Collinson J.D. (1996) - Clastic Coasts. Sedimentary Environments. Processes, Facies and Stratigraphy. Blackwells, Cornwall, 154-231.

Ricci Lucchi F. (1986) The Oligocene to Recent foreland basins of the northern Apennines. In: Allen P.A. & Homewood P. (Eds), Foreland Basins, Blackwell, Freiburg. 105-140. https://doi.org/10.1002/9781444303810.ch6.

Ricci Lucchi, F. (1995). Sedimentographica: Photographic atlas of sedimentary structures. Second edition. Columbia University Press, 255 pp.

Rousse S., Duringer P. & Stapf K.R.G. (2012) - An exceptional rocky shore preserved during Oligocene (Late Rupelian) transgression in the Upper Rhine Graben (Mainz Basin, Germany). *Geological Journal*, 47: 388-408.

Sabbatini A., Negri A., Bartolini A., Morigi C., Boudouma O., Dinelli E., Florindo F., Galeazzi R., Holzmann M., Lurcock P. C., Massaccesi L., Pawlowski J. & Rocchi S. (2016) - Selective zircon accumulation in a new benthic foraminifer, *Psammophaga zirconia*. sp. nov. *Geobiology*, 14: 404-416. https://doi.org/10.1111/gbi.12179.

Saul G., Naish T.R., Abbott S.T. & Carter, R.M. (1999) - Sedimentary cyclicity in the marine Pliocene-Pleistocene of the Wanganui basin (New Zeland): Sequence stratigraphic motif characteristic of the Part 2.5 m.y. *Geological Society of America Bullettin*, 111: 524-537. https://doi.org/10.1130/0016-7606(1999)111<0524:SCITMP>2.3.CO;2.

Seers T.D., Sheharyar A., Tavani S. & Corradetti A. (2022) - Virtual outcrop geology comes of age: the application of consumer-grade virtual reality hardware and software to digital outcrop data analysis. *Computer & Geosciences*, 159: 105006. https://doi.org/10.1016/j.cageo.2021.105006.

Servizio Geologico d'Italia (2025). Carta Geologica d'Italia alla scala 1:50.000, F. 326 Ascoli Piceno. ISPRA. https://doi.org/10.15161/oar.it/at9v3-7ak89.

Sømme T.O., Helland-Hansen W., Martinsen O.J. & Thurmond J.B. (2009) - Relationships between morphological and sedimentological parameters in source-to-sink systems: a basis for predicting semi-quantitative characteristics in subsurface systems. *Basin Research*, 21: 361-387. https://doi.org/10.1016/j.sedgeo.2018.06.007.

Stalder N.F., Fellin M.G., Caracciolo L., Guillong M., Winkler W., Milli S., Moscatelli M. & Critelli S. (2018) - Dispersal pathways in the early Messinian Adriatic foreland and provenance of the Laga Formation (Central Apennines, Italy). *Sedimentary Geology*, 375: 289-308. https://doi.org/10.1016/j.sedgeo.2017.09.016.

Swift D.J.P. (1968) - Coastal erosion and transgressive stratigraphy. *Journal of Geology*, 76: 444-456. https://doi.org/10.1086/627342.

Taylor A.M. & Goldring R. (1993) - Description and analysis of bioturbation and ichnofabric. *Journal of the Geological Society*, *London*, 150: 141-148. https://doi.org/10.1144/gsjgs.150.1.0141.

Thiele S.T., Grose L., Samsu A., Micklethwaite S., Vollgger S.A., Cruden A.R. (2017) - Rapid, semi-automatic fracture and contact mapping for point clouds, images and geophysical data. *Solid Earth*, 8: 1241-1253. https://doi.org/10.5194/se-8-1241-2017.

Tozer R.S.J., Butler R.W.H., Chiappini M., Corrado S., Mazzoli S. & Speranza F. (2006) - Testing thrust tectonic models at mountain fronts: where has the displacement gone? *Journal of the Geological Society, London*, 163: 1-14. https://doi.org/10.1144/0016-764904-140.

Trincardi F., Correggiari A. & Roveri M. (1994) - Late Quaternary transgressive erosion and deposition in a modern epicontinental shelf: the Adriatic semienclosed basin. *Geo-Marine Letters*, 14: 41-51. https://doi.org/10.1007/BF01204470

van der Meulen M.J., Buite S.J.H., Meulenkamp J.E. & Wortel M.J.R. (2000) - An early Pliocene uplift of the central Apenninic foredeep and its geodynamic significance. *Tectonics*, 19: 300-313. https://doi.org/10.1029/1999TC900064.

van der Meulen M.J., Meulenkamp J.E. & Wortel M.J.R. (1998) - Lateral shifts of Apenninic foredeep depocentres reflecting detachment of subducted lithosphere. *Earth and Planetary Science Letters*, 154: 203-219. https://doi.org/10.1016/S0012-821X(97)00166-0.

Van Loon A.J., Moretti M., Tropeano M., Acquafredda P., Baldacconi R., Festa V., Lisco S., Mastronuzzi G., Moretti V. & Scotti R. (2017) - Tracing the Source of the Bio/Siliciclastic Beach Sands at Rosa Marina (Apulian Coast, SE Italy). In: Mazumder R. (Ed) - Sediment Provenance:

Influences on Compositional Change from Source to Sink. Elsevier, pp. 25-47. https://doi.org/10.1016/B978-0-12-803386-9.00003-4.
Valloni R., Cipriani N. & Morelli C. (2002) - Petrostratigraphic record of the Apennine foredeep basins, Italy. *Bollettino della Società Geologica Italiana*, Spec. Vol. 1: 455-465.
WoRMS Editorial Board (2026). World Register of Marine Species. Available from https://www.marinespecies.org at VLIZ. Accessed 2026-06-01. https://doi.org/10.14284/170.
Zecchin M. & Caffau M. (2012) - The vertical compartmentalization of reservoirs: An example from an outcrop analog, Crotone Basin, southern Italy. *AAPG Bulletin*, 96: 155-175. https://doi.org/10.1306/05161110120.
Zecchin M., Caffau M. & Catuneanu O. (2021) - Recognizing maximum flooding surfaces in shallow-water deposits: an integrated sedimentological and micropaleontological approach (Crotone Basin, southern Italy). *Marine and Petroleum Geology*, 133: 105225. https://doi.org/10.1016/j.marpetgeo.2021.105225.
Zecchin M., Caffau M. & Catuneanu O. (2022) - Identification of maximum flooding surfaces at different scales: the case of the Piacenzian to Gelasian Cutro Clay and Strongoli sandstone (Crotone Basin, southern Italy). *Marine and Petroleum Geology*, 146: 105971. https://doi.org/10.1016/j.marpetgeo.2022.105971.
Zecchin M., Caffau M. & Catuneanu O. (2025a) - Milankovitch- and millennial-scale sequences in the late Piacenzian to early Gelasian shelf succession of the Crotone Basin, southern Italy. *Geosciences*, 15: 210. https://doi.org/10.3390/geosciences15060210.
Zecchin M., Caffau M., Catuneanu O. & Lenaz D. (2017) - Discrimination between wave-ravinement surfaces and bedset boundaries in Pliocene shallow-marine deposits, Crotone Basin, southern Italy: an integrated sedimentological, micropalaeontological and mineralogical approach. *Sedimentology*, 64: 1755-1791. https://doi.org/10.1111/sed.12373.
Zecchin M. & Catuneanu O. (2013) - High-resolution sequence stratigraphy of clastic shelves I: Units and bounding surfaces. *Marine and Petroleum Geology*, 39: 1-25. https://doi.org/10.1016/j.marpetgeo.2012.08.015.
Zecchin M. & Catuneanu O. (2017) - High-resolution sequence stratigraphy of clastic shelves VI: Mixed siliciclastic-carbonate systems. *Marine and Petroleum Geology*, 88: 712-723. http://dx.doi.org/10.1016/j.marpetgeo.2017.09.012.
Zecchin M., Catuneanu O. & Caffau M. (2019) - Wave-ravinement surfaces: Classification and key characteristics. *Earth-Science Reviews*, 188: 210-239. https://doi.org/10.1016/j.earscirev.2018.11.011.
Zecchin M., Catuneanu O. & Caffau M. (2024) - Zanclean to Gelasian high-frequency sequences of the Crotone basin (southern Italy): architectural variability and forcing mechanisms. *Marine and Petroleum Geology*, 162: 106753. https://doi.org/10.1016/j.marpetgeo.2024.106753.
Zecchin M., Catuneanu O. & Caffau M. (2025b) - Sequence stratigraphy of wave-dominated and wave-influenced shoreface deposits: systems tracts, stratigraphic surfaces and facies contacts. *Sedimentary Geology*, 489: 106980. https://doi.org/10.1016/j.sedgeo.2025.106980.

Appendix 1

Paleoenvironmental and paleoecological significance of the invertebrate assemblage

The invertebrate assemblage recovered from the Spungone Sandstone constitutes a taxonomically diverse and paleontologically informative multi-guild marine benthic community providing a high-resolution window into a Pliocene Mediterranean shallow-water ecosystem. A total of 63 invertebrate taxa have been identified, spanning seven major groups: Bivalvia, Gastropoda, Rhynchonellata (brachiopods), Anthozoa (solitary corals), Thecostraca (barnacles), and Echinoidea (irregular echinoids). Among these, approximately 55% represent extant species or genera with well-constrained ecological tolerances, providing robust analogues for paleoenvironmental reconstruction. The remaining taxa are extinct forms whose paleoecological significance can be inferred through phylogenetic and functional morphological comparisons with their closest living relatives.

The taxonomic composition, ecological structure, and taphonomic features indicate deposition within a dynamic mixed siliciclastic-bioclastic shelf system characterized by strong spatial heterogeneity in substrate type and variable hydrodynamic energy. The abundance of pectinids (e.g., *Aequipecten opercularis*, *Pecten jacobaeus*, *Lissochlamys* spp.) and venerids (e.g., *Chamelea gallina*, *Callista chione*, *Dosinia lupinus*) indicates well-oxygenated, fully marine conditions developed on biodetrital or sandy bottoms under moderate energy regimes, consistent with infralittoral to upper circalittoral environments (Ragaini & Mariani 1992; Dominici & Forli 2021; Marquet & Dijkstra 2000). In particular, *Chamelea gallina* (Weber & Zuschin 2013), *Glycymeris nummaria* (Legac & Hrs-Brenko 1999) and *Neverita olla* (Huelsken et al. 2008) are characteristic of sandy bottoms in the shoreface, indicating normal marine salinity and 10-20 m depth. In contrast, the co-occurrence of infaunal taxa adapted to fine-grained, low-energy substrates, including *Glossus humanus*, *Varicorbula gibba*, *Lutraria* spp., *Anadara gibbosa*, and deep-burrowing forms such as *Panopea glycimeris*, indicates the development of mixed sandy-muddy microhabitats within the same depositional system, reflecting pronounced facies variability and environmental patchiness (Dominici 2001; Cau et al. 2019).

From a paleoclimatic perspective, the assemblage contains a significant proportion of thermophilic and warm-water taxa, including *Procardium diluvianum*, *Callista italica, Circomphalus foliaceolamellosus*, *Malea orbiculata*, *Conus* sp., *Solatia piscatoria*, and *Architectonica* sp., which collectively indicate that the fossil assemblage was deposited during a warm phase characterized by sea surface temperatures comparable to or warmer than present-day Mediterranean values. This faunal composition is consistent with the broader interpretation of the Pliocene Mediterranean as a warm sea characterized by reduced meridional thermal gradients and enhanced faunal exchange with subtropical and tropical provinces (Monegatti & Raffi 2001; Scarponi et al. 2014; Pimentel et al. 2025). The occurrence of extinct or stratigraphically constrained taxa, such as *Callista italica*, *Pecten flabelliformis*, and *Pelecyora brocchii*, provides robust biostratigraphic support for a Pliocene age assignment and enables correlation with established Mediterranean shallow-marine reference sections (Monegatti & Raffi 2001; Cau et al. 2019; Mondanaro et al. 2024).

The trophic structure of the molluscan assemblage is characterized by a heterogeneous shallow-marine community dominated by suspension-feeding bivalves, accompanied by a subordinate but ecologically significant component of grazing, deposit-feeding, scavenging, and predatory gastropods. Overall, the association reflects a well-oxygenated, nutrient-rich infralittoral to circalittoral soft-bottom environment with relatively high primary productivity and abundant suspended organic matter. Suspension feeders clearly dominate the assemblage. Pectinids, together with ostreids, mytilids, limids, arcoids, and most venerids, were epifaunal or shallow infaunal filter feeders exploiting suspended phytoplankton and organic particles from the water column. The abundance and diversity of these taxa indicate persistent water circulation and elevated trophic resources, likely sustained by moderate hydrodynamic activity capable of maintaining food particles in suspension. The occurrence of large sessile forms, such as *Ostrea edulis*, *Chama gryphoides*, and the barnacle *Concavus concavus*, and anchor-living bivalves, such as *Atrina fragilis*, further supports the presence of stable substrates (i.e., conglomeratic lags and bioclastic shell pavements) locally available within predominantly sandy bottoms.

Infaunal suspension feeders are also particularly abundant. Taxa such as *Chamelea gallina*, *Dosinia lupinus*, *Polititapes vetulus*, *Pelecyora brocchii*, and *Lutraria* spp. inhabited sandy substrates where they filtered suspended matter through siphonal activity. The common occurrence of articulated *Panopea glycimeris* preserved in upright life position suggests low rates of post-mortem transport and indicates stable soft substrates suitable for deep-burrowing suspension feeders. The coexistence of shallow and deep infaunal taxa points to a tiered benthic ecosystem with efficient exploitation of trophic resources within the sediment-water interface.

Deposit-feeders are represented by taxa such as *Scaphander lignarius* and some turritellids, which likely consumed organic-rich sediment particles and microbial films. Their presence indicates the accumulation of benthic organic matter within the substrate. Similarly, *Varicorbula gibba*, an opportunistic species tolerant of elevated organic input, may reflect episodic increases in nutrient availability and sediment instability.

Gastropods document a wide spectrum of trophic strategies. Predatory and scavenging taxa, including *Conus* sp., *Semicassis saburon*, *Malea orbiculata*, *Tritia mutabilis*, and naticids such as *Cochlis raropunctata* and *Sinum striatum*, indicate the availability of abundant benthic prey. *Epitonium* sp. and *Eglisia spirata* may have functioned as specialized predators or ectoparasites, likely associated with cnidarians and other invertebrates. The occurrence of *Architectonica* sp. and cypraeids suggests additional grazing or microcarnivorous ecological niches. Altogether, the gastropod assemblage indicates a structurally complex food web with multiple trophic levels.

Irregular echinoids of the genus *Schizaster* are infaunal deposit feeders that burrow through soft, organic-rich sediments. Modern and fossil schizasterids are characteristic of low-energy, soft-bottom environments, typically 20-200 m, where they feed on organic detritus in fine sandy to muddy sediments.

References

Cau S., Laini A., Monegatti P., Roveri M., Scarponi D. & Taviani M. (2019) - Palaeoecological anatomy of shallow-water

Plio-Pleistocene biocalcarenites (Northern Apennines, Italy). *Palaeogeography, Palaeoclimatology, Palaeoecology*, 514: 838-851. https://doi.org/10.1016/j.palaeo.2018.08.011.

Dominici S. (2001) - Taphonomy and paleoecology of shallow marine macrofossil assemblages. *Palaios*, 16: 336-353. https://doi.org/10.1669/0883-1351(2001)016<0336:TAPOSM>2.0.CO;2.

Dominici S. & Forli M. (2021) - Lower Pliocene molluscs from southern Tuscany (Italy). *Bollettino della Società Paleontologica Italiana*, 60: 69-98. https://doi.org/10.4435/BSPI.2021.04.

Huelsken T., Marek C., Schreiber S., Schmidt I. & Hollmann M. (2008) - The Naticidae (Mollusca: Gastropoda) of Giglio Island (Tuscany, Italy): Shell characters, live animals, and a molecular analysis of egg masses. *Zootaxa*, 1770: 1-40.

Legac M. & Hrs-Brenko M. (1999). A review of bivalve species in the eastern Adriatic sea. III. Pteriomorpha (Glycymerididae). *Natura Croatica*, 8: 9-25.

Marquet R. & Dijkstra H.H. (2000) - Pliocene species of *Aequipecten* (Mollusca, Bivalvia, Pectinidae) from the North Sea Basin. *Contributions to Tertiary and Quaternary Geology*, 37: 39-55.

Mondanaro A., Dominici S. & Danise S. (2024) - Response of Mediterranean Sea bivalves to Pliocene-Pleistocene environmental changes. *Palaeontology*, 67: 12696. https://doi.org/10.1111/pala.12696.

Monegatti P. & Raffi S. (2001) - Taxonomic diversity and stratigraphic distribution of Mediterranean Pliocene bivalves. *Palaeogeography, Palaeoclimatology, Palaeoecology*, 165: 171-193. https://doi.org/10.1016/S0031-0182(00)00159-0.

Pimentel R.J., Callapez P.M., Pai M., Legoinha P. & Dinis P.A. (2025) - Pliocene marine Bivalvia from Vale Farpado (Pombal, Portugal): palaeoenvironmental and palaecological significance. *Geosciences*, 15: 309. https://doi.org/10.3390/geosciences15080309.

Ragaini, L. & Mariani R. (1992) - Analisi paleoecologica della malacofauna pliocenica di Camino Tondo (Grosseto, Italia). *Atti Società Toscana di Scienze Naturali, Mem., Serie A*, 99: 1-27.

Weber K. & Zuschin M. (2013) - Delta-associated molluscan life and death assemblages in northern Adriatic Sea: Implications for paleoecology, regional diversity and conservation. *Palaeogeography, Palaeoclimatology, Palaeoecology*, 370: 77-91. https://doi.org/10.1016/j.palaeo.2012.11.021.